

NEUTRINO ASTROPHYSICS

W. C. Haxton

Institute for Nuclear Theory and Department of Physics
 Box 351550 University of Washington, Seattle, WA 98195
 email: Haxton@phys.washington.edu

1 Introduction

The neutrino [1] is an elementary particle that scatters only through the weak interaction, and consequently rarely interacts in matter. Neutrinos are neutral, carry spin-1/2, and are members of the family of elementary particles called leptons. Thus they differ from the quarks of the standard model (spin-1/2 particles which participate in strong and electromagnetic interactions) and from the other leptons, which are charged and thus interact electromagnetically. Neutrinos and their antiparticles come in three types – or flavors – labeled according to the charged partners, the electron, muon, or tauon, that accompany neutrino production in charge-changing weak interactions. The most familiar such reaction is β decay

$$(N, Z) \rightarrow (N - 1, Z + 1) + e^- + \bar{\nu}_e$$

in which a nucleus containing N neutrons and Z protons decays to a lighter nucleus by converting a neutron to a proton, with the emission of an electron and an electron antineutrino. Indeed, it was the apparent absence of energy conservation in nuclear β decay that first lead Wolfgang Pauli, nearly 80 years ago, to suggest that some undetected neutral particle (the ν_e) must be escaping from nuclear β decay experiments.

Neutrinos play a very special role in astrophysics [2]. First, they are the direct byproducts of the nuclear reaction chains by which stars generate energy: each solar conversion of four protons into helium produces two neutrinos, for a total of $\sim 2 \times 10^{38}$ neutrinos each second. The resulting flux is observable on Earth. These neutrinos carry information about conditions deep in the solar core, as they typically leave the Sun without further interacting. They also provide experimentalists with opportunities for testing the properties of neutrinos over long distances. Second, they are produced in nature's most violent explosions, including the Big Bang, core-collapse supernovae, and the accretion disks encircling supermassive black holes. Recent discoveries of neutrino mass show that neutrinos comprise a small portion of the “dark matter” that influences how large-scale structure – the pattern of voids and galaxies mapped by astronomers – formed over cosmological times. Third, they dominate the cooling of many astrophysical objects, including young neutron stars and the degenerate helium cores of red giants. Neutrinos can be radiated from deep within such bodies, in contrast to photons, which are trapped within stars, diffusing outward only slowly. Finally, neutrinos are produced in our atmosphere and elsewhere as secondary byproducts of cosmic-ray collisions. Diagnosis of these neutrinos can help constrain properties of the primary cosmic ray spectrum.

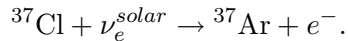
Neutrinos also mediate important astrophysical processes. The supernova “neutrino wind,” which blows off the surface of the proto-neutron star just seconds after core collapse, is thought to produce conditions favorable for the synthesis of about half of the neutron-rich nuclear species

heavier than iron, through rapid neutron capture (the r-process). Neutrinos also directly synthesize certain rare nuclei, such as ^{19}F .

Nuclear and particle physicists are exploiting astrophysical neutrino fluxes to do important tests of the standard model of particle physics. These tests include neutrino oscillations (the process by which a massive neutrino can be produced in one flavor state but detected later as a neutrino with a different flavor), neutrino decay, neutrino mass effects, and searches for nonzero neutrino electromagnetic moments.

2 Solar Neutrinos

The first successful effort to detect neutrinos from the Sun began four decades ago. Ray Davis, Jr. and his collaborators constructed a 650-ton detector in the Homestake Gold Mine, one mile beneath Lead, South Dakota [3]. This radiochemical detector, based on the chlorine-bearing cleaning fluid C_2Cl_4 , was designed to capture about one of the approximately 10^{18} high-energy neutrinos that penetrated it each day – the rest passed through the detector, without interacting. The neutrino-capture reaction was inverse-electron-capture



The product of this reaction, ^{37}Ar , is a noble gas isotope with a half life of about one month. It can be efficiently removed from a large volume of organic fluid by a helium gas purge, then counted in miniature gas proportional counters as ^{37}Ar decays back to ^{37}Cl . Davis typically exposed his detector for about two months, building up to nearly the saturation level of a few dozen argon atoms, then purged the detector to determine the number of solar neutrinos captured during this period.

Within a few years it became apparent that the number of neutrinos detected was only about one-third that predicted by the standard solar model (SSM) [4, 5], that is, the model of the Sun based on the standard theory of main sequence stellar evolution. Some initially attributed this “solar neutrino problem” to uncertainties in the SSM: As the flux of neutrinos most important to the Davis detector vary as $\sim T_c^{22}$, where T_c is the solar core temperature, a 5% theory uncertainty in T_c could explain the discrepancy. In fact, the correct explanation for the discrepancy proved much more profound. Davis was awarded the 2002 Nobel Prize in Physics for the Cl experiment.

During the three-decade period of ^{37}Cl detector operations, five other solar neutrino experiments were constructed. The SAGE and GALLEX/GNO experiments, radiochemical detectors similar to Cl, but using ^{71}Ga as a target, were designed to measure the flux of neutrinos from the dominant low-energy branch of solar neutrinos, the pp neutrinos. The first detector to measure neutrinos event by event, recording neutrino interactions in real time, was the converted proton decay detector Kamiokande. The detector contained three kilotons of very pure water, with solar neutrinos scattering off the electrons within the water. Phototubes surrounding the tank recorded the ring of Cerenkov radiation produced by the recoiling relativistic electrons. Kamiokande measured the high-energy neutrinos most important to the Davis detector, and thus confirmed the deficit that Davis had originally observed. Finally, a new generation of massive water (Super-Kamiokande) and heavy-water (Sudbury Neutrino Observatory (SNO)) detectors were constructed. The later, in a most direct way, showed that solar neutrinos were not missing, but rather hidden by a change of flavor occurring during their transit from the Sun to the Earth – as will be described later in this chapter.

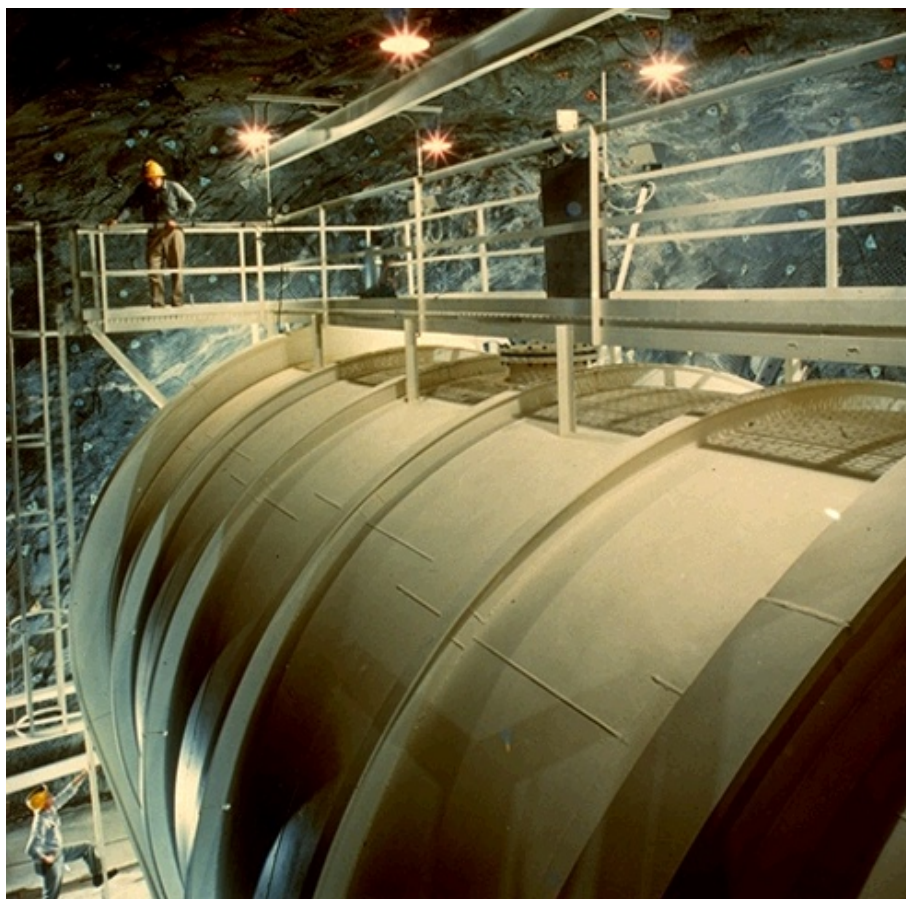
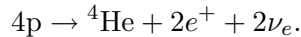


Figure 1: The Homestake Mine's chlorine detector, which Ray Davis Jr. and colleagues operated for over three decades.

2.1 The Standard Solar Model

The Sun belongs to a class of “main sequence” stars that derive their energy from burning protons to He in their cores. The SSM employs the standard theory of main-sequence stellar evolution, calibrated by the many detailed measurements only possible for the Sun, to follow the Sun from the onset of thermonuclear reactions 4.6 b.y. ago to today, thereby determining the present-day temperature and composition profiles of the solar core. These profiles govern solar neutrino production and other properties of the modern Sun. The SSM is based on four basic assumptions:

- The Sun evolves in hydrostatic equilibrium, maintaining a local balance between the gravitational force and the pressure gradient. To describe this condition in detail, one must specify the electron-gas equation of state as a function of temperature, density, and composition.
- Energy is transported by radiation and convection. While the solar envelope is convective, radiative transport dominates in the core region where thermonuclear reactions take place. The radiative opacity depends sensitively on the solar composition, particularly the abundances of heavier elements.
- Thermonuclear reaction chains generate solar energy. The standard model predicts that 99% of this energy is produced from the pp chain conversion of four protons into ${}^4\text{He}$ (see Fig. 2)



The Sun is a large but slow reactor: the core temperature, $T_c \sim 1.5 \times 10^7$ K, results in typical center-of-mass energies for reacting particles of ~ 10 keV, much less than the Coulomb barriers inhibiting charged particle nuclear reactions. Thus reaction cross sections are small: in most cases, as laboratory measurements are only possible at higher energies, cross section data must be extrapolated to the solar energies of interest.

- The model is constrained to produce today’s solar radius, mass, and luminosity. An important assumption of the SSM is that the Sun was highly convective, and therefore uniform in composition, when it first entered the main sequence. It is furthermore assumed that the surface abundances of metals (nuclei with $A > 5$) were undisturbed by the subsequent evolution, and thus provide a record of the initial solar metallicity. The remaining parameter is the initial ${}^4\text{He}/\text{H}$ ratio, which is adjusted until the model reproduces the present solar luminosity after 4.6 billion years of evolution. The resulting ${}^4\text{He}/\text{H}$ mass fraction ratio is typically 0.27 ± 0.01 , which can be compared to the Big-Bang value of 0.23 ± 0.01 . Note that the Sun was formed from previously processed material.

Three cycles with quite different temperature dependences, reflecting the relative ease or difficulty of Coulomb barrier penetration, comprise the pp chain of Fig. 2. The competition between the cycles is very sensitive to the solar core temperature T_c . The initial interest in solar neutrinos came from the observation that each of the three cycles is associated with a characteristic neutrino. Thus, by measuring solar neutrinos, specifically the pp, ${}^7\text{Be}$, and ${}^8\text{B}$ neutrinos, one can determine the relative importance of the ppI, ppII, and ppIII cycles, and consequently determine T_c to an accuracy approaching 1%.

The neutrino-producing reactions of the pp chain and CN cycle (a second process for burning protons to He, dominant in massive main-sequence stars, but responsible for only $\sim 1\%$ of solar

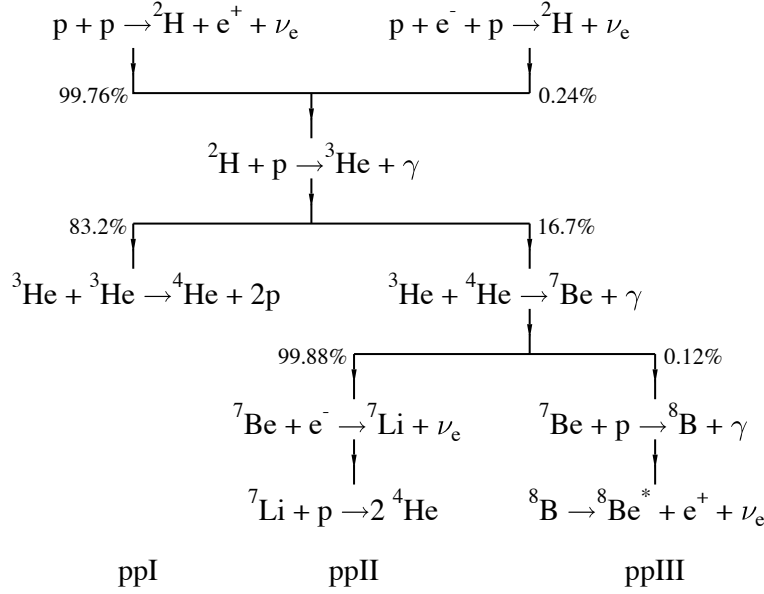


Figure 2: The pp-chain for hydrogen burning. The relative rates of competing reactions correspond to the Bahcall-Pinsonneault 2004 SSM [6].

energy) are summarized in Table 1. The first six reactions are β decays that produce continuous neutrino spectra. The last two reactions produce line sources of electron capture neutrinos, with widths ~ 2 keV characteristic of the temperature of the solar core. Table 1 gives the predicted fluxes of these neutrinos at Earth, as determined in two SSM calculations, Bahcall, Serenelli, and Basu (BS05(AGS,OP) [4] and Brun, Turk-Chieze, and Morel (BTCM98) [5]. An update of the BS05(AGS,OP) SSM is in progress.

2.2 SNO and Super-Kamiokande

Solar neutrino detection requires the combination of a large detector volume (to provide the necessary rate of events), very low backgrounds (so that neutrino events can be distinguished from backgrounds due to cosmic rays and natural radioactivity), and a distinctive signal. The first requirement favors detectors constructed from inexpensive materials and/or materials having large cross sections for neutrino capture. The second generally requires a deep-underground location for the detector, with sufficient rock overburden to attenuate the flux of penetrating muons produced by cosmic ray interactions in the atmosphere. It also requires very careful attention to detector cleanliness, including tight limits on dust or other contaminants that might introduce radioactivity, use of low-background construction materials, control of radon, and often the use of fiducial volume cuts so that the outer portions of a detector become a shield against activities produced in the surrounding rock walls.

There are several possible detection modes for solar neutrinos, interesting because of their different sensitivities to flavor. The early radiochemical experiments using ${}^{37}\text{Cl}$ and ${}^{71}\text{Ga}$ targets

Table 1: Solar neutrino sources and the flux predictions of the Bahcall, Serenelli, and Basu BS05(AGS,OP) [4] and the Brun, Turk-Chieze, and Morel BTCM98 [5] SSMs. The former uses abundances derived from recent re-analyses of photospheric absorption lines and new opacities from the Opacity Project.

Source	E_ν^{max} (MeV)	BS05(AGS,OP) ($\text{cm}^{-2} \text{ s}^{-1}$)	BTCM98 ($\text{cm}^{-2} \text{ s}^{-1}$)
$p + p \rightarrow {}^2\text{H} + e^+ + \nu$	0.42	6.06×10^{10}	5.98×10^{10}
${}^{13}\text{N} \rightarrow {}^{13}\text{C} + e^+ + \nu$	1.20	2.01×10^8	4.66×10^8
${}^{15}\text{O} \rightarrow {}^{15}\text{N} + e^+ + \nu$	1.73	1.45×10^8	3.97×10^8
${}^{17}\text{F} \rightarrow {}^{17}\text{O} + e^+ + \nu$	1.74	3.25×10^6	
${}^8\text{B} \rightarrow {}^8\text{Be} + e^+ + \nu$	~ 15	4.51×10^6	4.82×10^6
${}^3\text{He} + p \rightarrow {}^4\text{He} + e^+ + \nu$	18.77	8.25×10^3	
${}^7\text{Be} + e^- \rightarrow {}^7\text{Li} + \nu$	0.86 (90%) 0.38 (10%)	4.34×10^9	4.70×10^9
$p + e^- + p \rightarrow {}^2\text{H} + \nu$	1.44	1.45×10^8	1.41×10^8

were based on the charged current weak reaction

$$\nu_e + (N, Z) \rightarrow e^- + (N - 1, Z + 1)$$

where the signal for neutrino absorption is the growth over time of very small concentrations of the daughter nucleus $(N - 1, Z + 1)$ in the detector. As the spectrum of solar neutrinos extends only to about 15 MeV, well below the threshold for producing muons, this reaction is sensitive only to electron neutrinos.

A second possible nuclear detection channel is neutral-current scattering

$$\nu_x + (N, Z) \rightarrow \nu'_x + (N, Z)^*,$$

a process independent of the neutrino flavor. If this scattering leaves the nucleus in an excited state, the observable would be the de-excitation of the nucleus, such as a decay γ ray or the breakup of the nucleus. (An example will be given below, in the discussion of SNO.) Alternatively, neutrino elastic scattering (without nuclear excitation) is a coherent process at low energies, with a cross section proportional to the square of the weak charge, which is approximately the neutron number N of the nucleus. The signal then is the small recoil energy of the nucleus after scattering.

A third possibility is the scattering of neutrinos off electrons,

$$\nu_x + e^- \rightarrow \nu'_x + e^-,$$

with detection of the recoiling scattered electron. Both electron- and heavy-flavor (ν_μ , ν_τ) solar neutrinos can scatter off electrons, the former by charge and neutral currents, and the latter by neutral currents only. Consequently the cross section for scattering heavy-flavor neutrinos is only

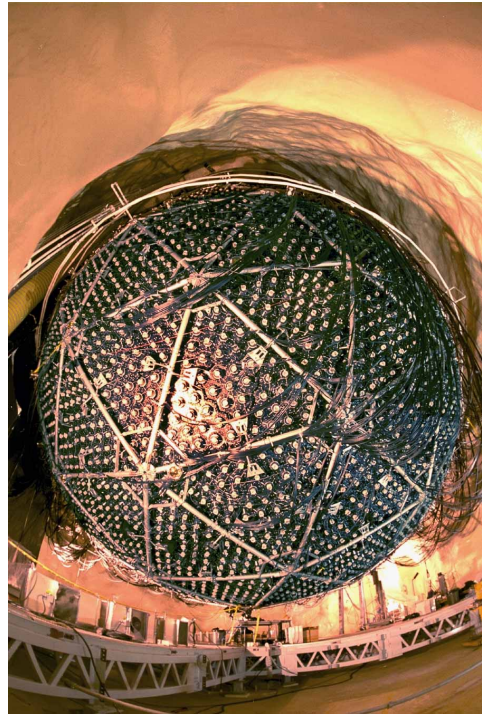
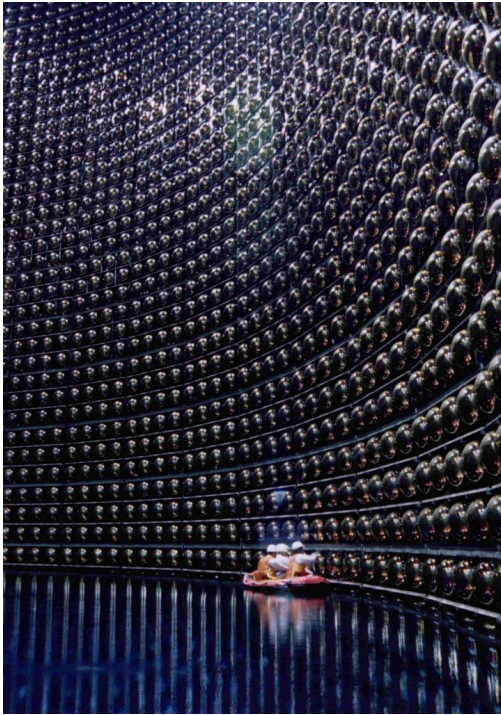


Figure 3: The left panel shows the Super-Kamiokande detector during filling, with scientists cleaning PMT surfaces as the water rises. The right panel is a fish-eye photo of the SNO detector and cavity, showing the PMTs and support structure prior to cavity and detector filling.

about 0.15 that for electron neutrinos. This process provides a third way of probing neutrino flavor, due to this differential sensitivity. An important aspect of electron-neutrino scattering is its directionality: for solar neutrino energies much above the electron mass of 0.511 MeV, the electron scatters into a narrow cone along the incident neutrino's direction. This directionality provides a powerful tool for extracting solar neutrino events from background: neutrino events correlate with the direction of the Sun, while background events should be isotropic. Thus neutrino events can be identified as the excess seen at forward electron angles.

These various detection channels were exploited in two large-volume water Cerenkov detectors that recorded events in real time and provided flavor sensitivity.

Super-Kamiokande (Fig. 3) is a detector consisting of 50 kilotons of ultra-pure water within a cylindrical stainless steel tank, 39m in diameter and 42m tall. Two meters inside the walls a scaffold supports a dense array of 50-cm-diameter hemispherical photomultiplier tubes (PMTs), which face inward and view the inner 32 kilotons of water. Additional 20-cm tubes face outward, viewing the outer portion of the detector that serves as a shield and as a veto. A solar neutrino can interact in the inner detector, scattering off an electron. The recoiling, relativistic electron then produces a cone of Cerenkov radiation, a pattern that can be reconstructed from the triggering of the phototubes that surround the inner detector. The detector is housed deep within Japan's Kamioka Mine, approximately one kilometer underground.

The detector has produced three data sets. In the first, obtained from 1996-2001, the detector was instrumented with an array of 11,146 50-cm PMTs, corresponding to about 40% coverage. In November 2001 one of the 50-cm PMTs imploded, creating a powerful shock wave that propagated through the tank, destroying 60% of the phototubes. The detector was subsequently rebuilt with about half the original number of phototubes, evenly spaced over the scaffold, so that the coverage was reduced to 20%. The detector operated in this SK-II phase in the years 2003-5. In August 2006 the detector resumed operations after a second reconstruction in which the phototube coverage was restored to 40% and other improvements made. This marked the start of the ongoing SK-III phase. The SK-I and SK-II results [7] for the high-energy ^8B neutrino flux are $(2.35 \pm 0.02(\text{stat}) \pm 0.08(\text{sys})) \times 10^6/\text{cm}^2\text{s}$ and $(2.38 \pm 0.05 \pm 0.16) \times 10^6/\text{cm}^2/\text{s}$, respectively, well below the SSM predictions of Table 1.

The Sudbury Neutrino Observatory (SNO) (Fig. 3) was constructed at quite extraordinary depth, two kilometers underground in Inco's Creighton nickel mine in Ontario, Canada. The detector took data from May 1999 through November 2006, operating in three different modes over its 7.5-year lifetime. SNO employed a one-kiloton target of heavy water, contained within a spherical acrylic vessel six meters in radius. This sphere was surrounded by an additional five meters (seven kilotons) of very pure ordinary water, filling the rock cavity that housed the entire detector. An array of 9600 20-cm PMTs, mounted on a geodesic sphere surrounding the inner vessel, provided 56% coverage. As in the case of Super-Kamiokande, SNO operated with a threshold of about 5 MeV. Thus it detected that portion of the ^8B solar neutrino spectrum from 5-15 MeV.

The choice of a heavy-water target allowed SNO experimentalists to exploit all three of the reaction channels described above, with their varying flavor sensitivities

$$\begin{array}{ll} \nu_x + e^- \rightarrow \nu'_x + e^- & \text{ES : elastic scattering} \\ \nu_e + d \rightarrow p + p + e^- & \text{CC : charged current} \\ \nu_x + d \rightarrow \nu'_x + n + p & \text{NC : neutral current} \end{array}$$

The elastic scattering (ES) reaction is the same as that employed by Super-Kamiokande, with its

differing sensitivities to electron- and heavy-flavor neutrinos. The charged-current (CC) reaction on deuterium is sensitive only to electron-flavor neutrinos, producing electrons that carry off most of the incident neutrino's energy (apart from the 1.44 MeV needed to break a deuterium nucleus into p+p). Thus, from the energy distribution of the electrons, one can reconstruct the incident ν_e spectrum (and possible distortions discussed below) more accurately than in the case of ES.

The NC reaction, which is observed through the produced neutron, provides no spectral information, but does measure the total solar neutrino flux, independent of flavor. The SNO experiment has used three techniques for measuring the neutrons. In the initial pure-D₂O phase the neutrons captured on deuterium, producing 6.25 MeV γ s. In a second phase 2.7 tons of salt were added to the heavy water so that Cl would be present to enhance the capture, producing 8.6 MeV γ s. In both of these approaches the NC and CC events can be separated reasonably well because of the modest backward peaking ($\sim 1-\cos\theta/3$) in the angular distribution of the latter. This allowed the experimenters to determine the total and electron neutrino fraction of the solar neutrino flux. Finally, in the third phase, direct neutron detection was provided in pure D₂O by an array of ³He-filled proportional counters, cleanly separating this signal from CC scattering.

SNO was constructed at very great depth and under clean-room conditions because of the need to suppress backgrounds. In particular, a minute amount of dust in the detector could have introduced environmental radioactivities that would have obscured the NC signal, a single neutron. The great advantage of the SNO detector was its three distinct detection channels, sensitive to different combinations of electron and heavy-flavor neutrinos. Furthermore, because the ES and CC scattered electrons are measured in the same detector, several important systematic effects cancel in the ratio of events. The ES reaction provided an important cross check on the consistency of the results from the CC and NC channel.

The first results [8] from SNO are shown in Fig. 4. The final SNO Phase I (neutron capture on deuterium) deduced fluxes are [9]

$$\begin{aligned}\phi_{CC} &= \left[1.76^{+0.06}_{-0.05}(\text{stat.})^{+0.09}_{-0.09}(\text{syst.}) \right] \times 10^6 / \text{cm}^2\text{s} \\ \phi_{ES} &= \left[2.39^{+0.24}_{-0.23}(\text{stat.})^{+0.12}_{-0.12}(\text{syst.}) \right] \times 10^6 / \text{cm}^2\text{s} \\ \phi_{NC} &= \left[5.09^{+0.44}_{-0.43}(\text{stat.})^{+0.46}_{-0.43}(\text{syst.}) \right] \times 10^6 / \text{cm}^2\text{s}\end{aligned}$$

Fig. 4 shows that the total flux (NC) is in agreement with the SSM prediction, but the neutrino flavor has been changed: about two-thirds of the electron neutrinos produced in the Sun arrive on Earth as heavy-flavor (muon or tauon) neutrinos. The Davis detector and the CC channel in SNO are blind to these heavy flavors, seeing only the portion with electron flavor. Thus the solar neutrino problem was not a matter of missing neutrinos, but rather one of neutrinos in hiding. The implications of this discovery – that neutrinos are massive and violate flavor – are profound, indicating that our standard model of particle physics is incomplete.

2.3 Neutrino Mass and Oscillations

The phenomenon by which a massive neutrino of one flavor changes into one of a second flavor is called neutrino oscillations. Neutrino oscillations have been shown to be responsible not only for the missing solar neutrinos in Davis's experiment, but also for the missing atmospheric neutrinos that will be discussed in the next chapter. Neutrino oscillations can be altered by the presence of matter or the presence of other neutrinos. For this reason, astrophysical “laboratories” for

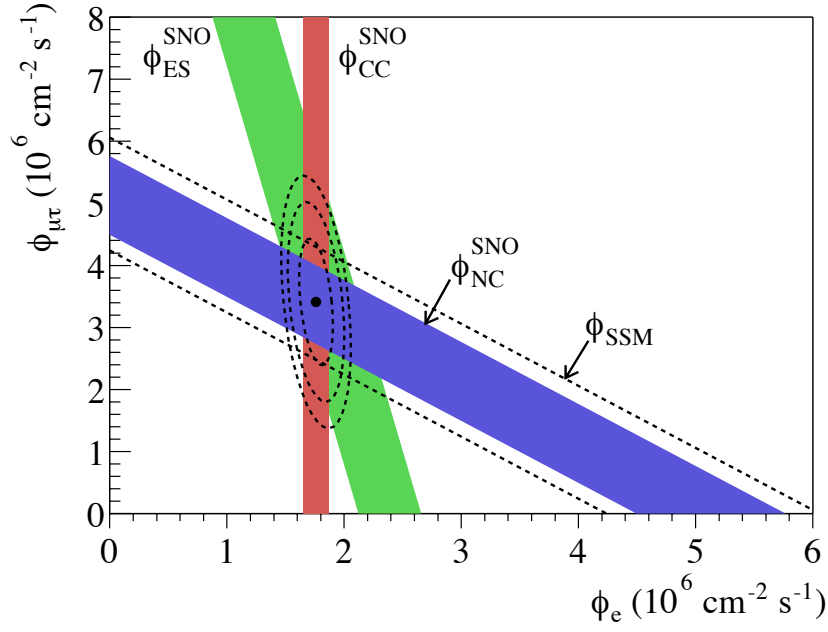


Figure 4: Results from the D₂O phase of the SNO experiment [9]. The allowed bands for CC, NC, and ES reactions of solar neutrinos intersect to show a flux that is one-third ν_e s and two-thirds heavy-flavor neutrinos. There is agreement between the NC total-flux measurement and the predictions of the SSM (band indicated by the dashed lines). Figure courtesy of the Sudbury Neutrino Observatory collaboration.

studying neutrinos – the Sun, supernovae, the early universe – are of great interest because of the unique conditions they provide, including very long “baselines” over which neutrino propagate and enormous matter densities and neutrino fluences.

Neutrino oscillations originate from two distinct sets of labels carried by neutrinos. One is flavor, a property of the weak interaction: an electron neutrino is defined as the neutrino accompanying a positron in β decay. The other possible label is mass. If a neutrino has a mass m , it propagates through free space with an energy and three momentum related by $\omega = \sqrt{\vec{k}^2 + m^2}$. Thus neutrino states can be labeled according to flavor, and also labeled according to their masses.

However nothing requires the neutrinos of definite flavor to be coincident with the neutrinos of definite mass. (In fact, in the analogous case of the quarks, it has long been known that the flavor (or weak interaction) eigenstates are not identical to the mass eigenstates: That is, the up quark decays not only to the down quark, but also occasionally to the strange quark.) Neutrino oscillations occur when the mass eigenstates $|\nu_1\rangle$ and $|\nu_2\rangle$ (with masses m_1 and m_2) are related to the weak interaction eigenstates by

$$\begin{aligned} |\nu_e\rangle &= \cos \theta_v |\nu_1\rangle + \sin \theta_v |\nu_2\rangle \\ |\nu_\mu\rangle &= -\sin \theta_v |\nu_1\rangle + \cos \theta_v |\nu_2\rangle \end{aligned}$$

where θ_v , the (vacuum) mixing angle, is nonzero. (Here, for simplicity, we consider just two neutrinos – the generalization to three flavors adds little new.)

In this case a state produced as a $|\nu_e\rangle$ or a $|\nu_\mu\rangle$ at some time t — for example, a neutrino produced in β decay in the Sun’s core — does not remain a pure flavor eigenstate as it propagates away from the source. The different mass eigenstates comprising the neutrino will accumulate different phases as the neutrino propagate downstream, a phenomenon known as vacuum oscillations (vacuum because the experiment is done in free space). While at time $t=0$ the neutrino is a flavor eigenstate

$$|\nu(t=0)\rangle = |\nu_e\rangle = \cos \theta_v |\nu_1\rangle + \sin \theta_v |\nu_2\rangle,$$

the accumulate phases depend on the mass

$$e^{i(\vec{k}\cdot\vec{x}-\omega t)} = e^{i[\vec{k}\cdot\vec{x}-\sqrt{m_i^2+k^2} t]}.$$

If the neutrino mass is small compared to the neutrino momentum/energy, one finds

$$|\nu(t)\rangle = e^{i(\vec{k}\cdot\vec{x}-kt-(m_1^2+m_2^2)t/4k)} \left(\cos \theta_v |\nu_1\rangle e^{i\delta m^2 t/4k} + \sin \theta_v |\nu_2\rangle e^{-i\delta m^2 t/4k} \right)$$

There is a common average phase (which has no physical consequence) as well as a beat phase that depends on

$$\delta m^2 = m_2^2 - m_1^2.$$

From this one can find the probability that the neutrino state remains a $|\nu_e\rangle$ at time t

$$P_{\nu_e}(t) = |\langle \nu_e | \nu(t) \rangle|^2 = 1 - \sin^2 2\theta_v \sin^2 \left(\frac{\delta m^2 c^4 x}{4\hbar c E} \right)$$

The probability oscillates from 1 to $1 - \sin^2 2\theta_v$ and back to 1 over an oscillation length scale

$$L_o = \frac{4\pi\hbar c E}{\delta m^2 c^4},$$

as depicted in Fig. 5. In the case of solar neutrinos, if L_o were comparable to or shorter than one astronomical unit, a reduction in the solar ν_e flux would be expected in terrestrial detectors.

The suggestion that the solar neutrino problem could be explained by neutrino oscillations was first made by Pontecorvo in 1958, who pointed out the analogy with $K_0 \leftrightarrow \bar{K}_0$ oscillations. If the Earth-Sun separation is much larger than L_o , one expects an average flux reduction due to oscillations of

$$1 - \frac{1}{2} \sin^2 2\theta_v.$$

For a 1 MeV neutrino, this requires $\delta m^2 c^4 \gg 10^{-12} \text{ eV}^2$. But such a reduction – particularly given the initial theory prejudice that neutrino mixing angles might be small – did not seem sufficient to account for the factor-of-three discrepancy that emerged from Davis’s early measurements.

The view of neutrino oscillations changed when Mikheyev and Smirnov [10] showed in 1985 that neutrino oscillations occurring in matter – rather than in vacuum – could produce greatly enhanced oscillation probabilities. This enhancement comes about because neutrinos propagating through matter acquire an additional mass due to their interactions with the matter. In particular, because the Sun contains many electrons, the electron neutrino becomes heavier in proportion to the local density of electrons. An enhanced probability for oscillations can result when an electron neutrino passes from a high-density region (such as the solar core) to a low-density one (such as the surface of the Earth). This matter enhancement is called the MSW mechanism after Mikheyev, Smirnov, and Wolfenstein [11] (who first described the phenomenon of neutrino effective masses).

To explain this enhancement, consider the case where the mixing angle in vacuum, θ_v , is small and $m_2 > m_1$. Then $|\nu_e\rangle \sim |\nu_1\rangle \equiv |\nu_L(\rho = 0)\rangle$ where ρ is the local electron density, that is, the ν_e and the light vacuum eigenstate $|\nu_L(\rho = 0)\rangle$ are almost identical. (Correspondingly, the heavy eigenstate $|\nu_2\rangle \equiv |\nu_H(\rho = 0)\rangle \sim |\nu_\mu\rangle$ in vacuum.) Now what happens in matter? As matter makes the ν_e heavier in proportion to the electron density, if that density is sufficiently high, clearly the electron neutrino must become the (local) heavy mass eigenstate. That is, $|\nu_e\rangle \sim |\nu_H(\rho \rightarrow \infty)\rangle$ (and consequently $|\nu_\mu\rangle \sim |\nu_L(\rho \rightarrow \infty)\rangle$). That is, we conclude that there must be a local mixing angle $\theta(\rho)$ that rotates from $\theta_v \sim 0$ in vacuum to $\theta(\rho) \sim \pi/2$ as $\rho \rightarrow \infty$.

MSW enhancement occurs when the density changes between neutrino production and detection. In particular, electron neutrinos produced in the high-density solar core are created as heavy mass eigenstates. If these neutrinos now propagate to the solar surface adiabatically – this means that changes in the solar density scale height $1/\rho \, d\rho/dx$ are small over an oscillation length, at all points along the neutrino trajectory – they will remain on the heavy-mass trajectory, and thus exit the Sun as $|\nu_H(\rho = 0)\rangle = |\nu_2\rangle \sim |\nu_\mu\rangle$. That is, there will be an almost complete conversion of the ν_e s produced in the solar core to ν_μ s. The MSW mechanism is an example of an avoided level crossing, a familiar phenomenon in quantum mechanics.

A schematic comparison of vacuum and matter-enhanced oscillations is shown in Fig. 5. The matter transition between electron and muon flavors is centered around a density where the vacuum mass difference is just compensated by the matter contributions.

The results from SNO and Super-Kamiokande, from earlier solar neutrino experiments, and from the reactor experiment KamLAND, have determined the parameters governing solar neutrino oscillations quite precisely [12]. Unlike the example given above, the relevant mixing angle is rather large, $\theta_{12} \sim 34^\circ$. The vacuum mass difference, $\delta m_{12}^2 \sim 7.94 \times 10^{-5} \text{ eV}^2$, leads to important matter effects in the higher energy portion of the solar neutrino spectrum, thus influencing the rates found in the SNO, Super-Kamiokande, and chlorine experiments. These effects produce a characteristic, energy-dependent distortion of the solar ν_e spectrum.

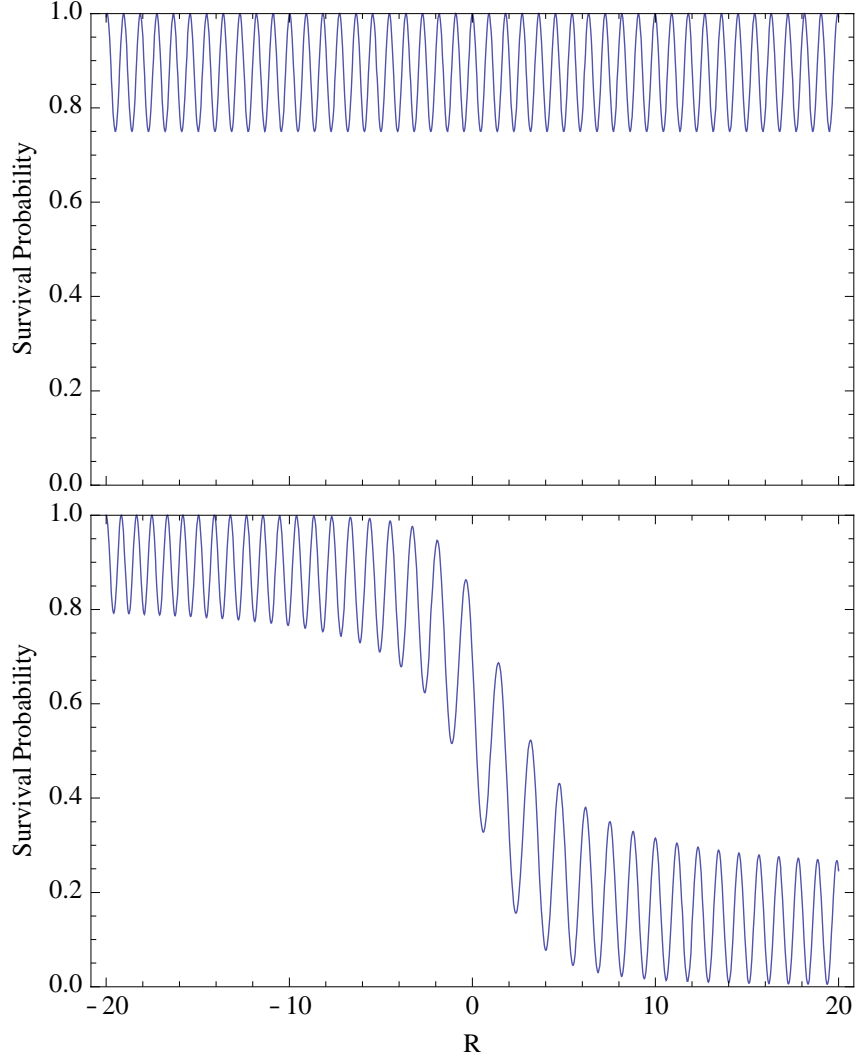


Figure 5: A simple example illustrating the MSW mechanism. The top frame shows vacuum oscillations for a ν_e created at $R = -20$ and propagating to the right, for $\theta_v = 15^\circ$. The average ν_e survival probability is large, 87.5%. (Here the distance R is given in units related to the oscillation length, $4E \cos 2\theta / (\delta m^2 \sin^2 2\theta)$.) In the bottom frame an electron density $\rho(R)$ has been added proportional to $1 - (2/\pi) \tan^{-1} aR$, with a chosen to guarantee adiabaticity, and normalized so that 1) $\rho(r) \rightarrow 0$ as $R \rightarrow \infty$; 2) the matter effects cancel the vacuum mass difference for $R \sim 0$ (the MSW crossing point); and 3) the matter effects reverse the sign of δm^2 as $R \rightarrow -\infty$. Thus these are the MSW conditions described in the text. A ν_e created at high density ($R = -20$), where it approximately coincides with the local heavy-mass eigenstate, adiabatically propagates to low-density ($R = +20$), where it approximately coincides with the ν_μ . Thus the ν_e survival probability at $R = 20$ is much reduced, compared to the vacuum case. Note that the local oscillation length is maximal near the crossing point.

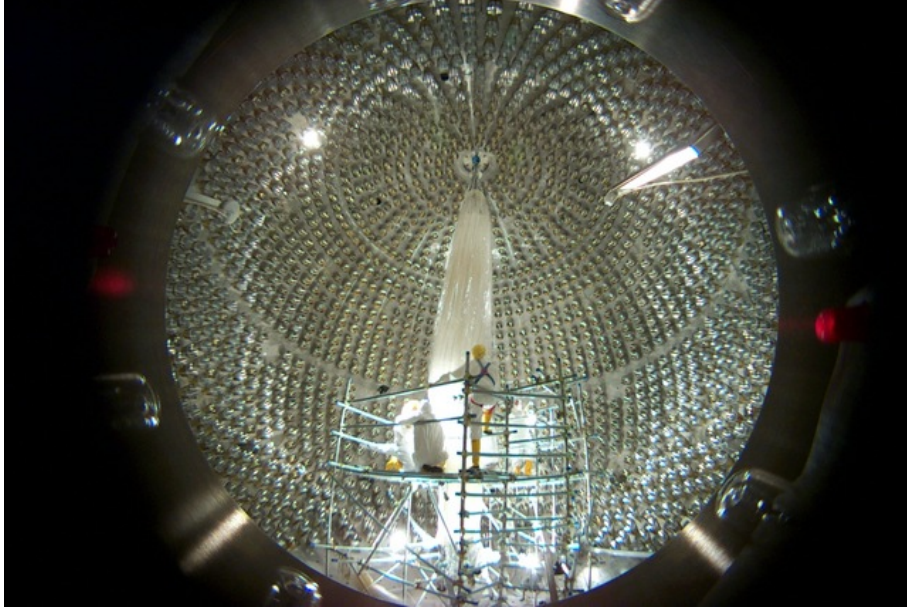


Figure 6: The Borexino inner vessel during installation.

2.4 Solar Neutrinos: Outlook

Neutrino oscillations proved to be responsible for both the solar neutrino problem and the atmospheric neutrino problem discussed in the next chapter. This phenomenon requires both flavor mixing and neutrino mass, phenomena that can be accommodated in various extensions of the standard model of particle physics. The great interest in neutrino astrophysics stems in part from the expectation that newly discovered neutrino properties may help us formulate the correct extension. Indeed, the tiny neutrino mass differences deduced from the solar and atmospheric problems are compatible with theories where the neutrino mass is inversely proportional to a scale for new physics of about 10^{15} GeV. This is close to the Grand Unified scale where supersymmetric extensions of the standard model predict that the strengths of the fundamental forces unify.

There remain important, unresolved issues in solar neutrino physics. The first direct (real-time) measurements of the dominant, low-energy neutrino fluxes – the pp and ^7Be neutrinos – are just beginning. Borexino [13], a scintillation detector operating in the Italy’s Gran Sasso laboratory (Fig. 6), began taking data on the ^7Be flux in May 2007. One goal is to test the prediction that the survival probability of ^7Be ν_e s will be larger than that for the higher energy neutrinos, since matter effects are more significant for the latter.

There are also interesting developments involving the SSM. One of the important validations of the SSM has come through helioseismology, the measurement of solar surface fluctuations, as deduced from the Doppler shifts of spectral lines. The observed patterns can be inverted to determine properties of interior acoustic and gravity waves, including the sound speed as a function of the solar radius. For about a decade the agreement between SSM predictions and observation had been excellent.

But recently improved three-dimensional models of photospheric absorption lines have led to a 30% downward revision in convective-zone metal abundances (that is, abundances of elements

heavier than helium). As discussed earlier, the SSM fixes the Sun’s zero-age metallicity to today’s surface abundances. If the new abundances are employed in the SSM, the resulting changes in the opacity alter both neutrino flux predictions and the sound speed profile. The discrepancy between the SSM sound speed profile and helioseismology is particularly significant in the Sun’s upper radiative zone. If this difficulty persists, some of the assumptions of the SSM, such as a homogeneous zero-age Sun, may have to be critically re-examined.

3 Atmospheric Neutrinos

The atmospheric neutrino problem developed very much in parallel with the solar neutrino problem and also involved missing neutrinos. The first definitive claim that neutrinos are massive came from the atmospheric neutrino group associated with Super-Kamiokande, in 1998. The oscillations seen in atmospheric neutrinos differ from those seen in solar neutrinos, resulting from the coupling of a different pair of neutrinos.

3.1 The Neutrino Source

When primary cosmic-ray protons and nuclei hit the upper atmosphere, the ensuing nuclear reactions with atmospheric oxygen and nitrogen nuclei produce secondaries such as pions, kaons, and muons. Atmospheric neutrinos arise from the decay of these secondaries. For energies less than ~ 1 GeV, the secondaries decay prior to reaching the Earth’s surface

$$\begin{aligned}\pi^\pm(K^\pm) &\rightarrow \mu^\pm + \nu_\mu(\bar{\nu}_\mu), \\ \mu^\pm &\rightarrow e^\pm + \nu_e(\bar{\nu}_e) + \bar{\nu}_\mu(\nu_\mu).\end{aligned}\tag{1}$$

Consequently one expects the ratio

$$r = (\nu_e + \bar{\nu}_e)/(\nu_\mu + \bar{\nu}_\mu)\tag{2}$$

to be approximately 0.5 in this energy range. Detailed Monte Carlo calculations, including the effects of muon polarization, give $r \sim 0.45$. This ratio should be rather insensitive to theoretical uncertainties. It does not depend on absolute fluxes, and as a ratio of related processes, one expects many sources of systematic error to cancel. Indeed, while various groups have estimated this ratio, sometimes starting with neutrino fluxes which vary in magnitude by up to 25%, agreement in the ratio has been found at the level of a few percent. This agreement persists at higher energies, where r decreases because higher energy muons survive passage through the atmosphere, due to the effects of time dilation.

Atmospheric neutrinos are a very attractive astrophysical source for experimenters. Apart from relatively minor geomagnetic effects, atmospheric neutrino production is uniform over the Earth. Thus an experimenter, operating an underground detector at some location, can make use of a set of nearly equivalent neutrino sources at distances ranging from 10s of kilometers (directly overhead) to 13,000 kilometers (directly below, produced on the opposite side of the Earth). Effects such as neutrino oscillations, which depend on the distance from the source to the target, might show up as a characteristic dependence of neutrino flux on the zenith angle, provided the relevant oscillation length is comparable to or less than the Earth’s diameter. (Note that the solar neutrino δm_{12}^2 , for atmospheric neutrinos of energy ~ 1 GeV, would not satisfy this condition, as the oscillation length is several times the Earth’s diameter.)

3.2 Atmospheric Neutrinos and Proton Decay Detectors

The atmospheric neutrino anomaly grew out of efforts to build large underground detectors for proton decay, one of the phenomena expected in the Grand Unified Theories that were formulated in the late 1970s and early 1980s. As atmospheric neutrinos and proton decay would deposit very similar energies in such detectors, studies of atmospheric neutrinos were a natural second use of such detectors. Significant indications of an anomaly came from the IMB [14] and Kamiokande [15] proton decay detectors. IMB first noticed a possible deficit of neutrino-induced muon events in 1986, while Kamiokande established a deficit in excess of 4σ by 1988. By 1998 this anomaly was also apparent in data from the Soudan detector and from Super-Kamiokande.

The quantity determined in such experiments is a ratio (observed to predicted) of ratios

$$R = \frac{(\nu_\mu/\nu_e)_{\text{data}}}{(\nu_\mu/\nu_e)_{\text{MonteCarlo}}}$$

where the numerator is determined experimentally, and the denominator calculated. Agreement between data and theory thus requires $R \sim 1$. Early experimenters faced a difficulty in evaluating this ratio due to limited statistics: the counting rates were too low to allow a detailed analysis based on the zenith angle, that is, based on the neutrino path length. This changed with the construction of Super-Kamiokande, which provided a fiducial volume of about 20 ktons. An early analysis from Super-Kamiokande found

$$R = 0.61 \pm 0.03(\text{stat}) \pm 0.05(\text{syst})$$

for sub-GeV events which were fully contained in the detector and

$$R = 0.66 \pm 0.05(\text{stat}) \pm 0.08(\text{syst})$$

for fully- and partially-contained multi-GeV events. In addition, the collaboration presented an analysis in 1998, based on 33 kton-years of data, showing a zenith angle dependence inconsistent with theoretical calculations of the atmospheric flux, in the absence of oscillations [16]. This indicated a distance dependence in the muon deficit, a signature of oscillations. Furthermore the parameters of the oscillation, especially $5 \times 10^{-4} \text{ eV}^2 < \delta m_{23}^2 < 6 \times 10^{-3} \text{ eV}^2$, differed from those that would later be determined from solar neutrinos. The collaboration concluded that the data were consistent with the two-flavor oscillation $\nu_\mu \rightarrow \nu_\tau$. This was the first definitive claim for massive neutrinos.

SK-I collected approximately 15,000 atmospheric neutrino events in nearly five years of running. The collaboration's zenith-angle analysis of the data found evidence of a first oscillation minimum at $L/E \sim 500 \text{ km/GeV}$, so that $L_o \sim 1000 \text{ km}$ for a 1 GeV muon neutrino. The full analysis of oscillation parameters (see Fig. 7) gives a best-fit δm_{23}^2 of 2.1×10^{-3} , a value clearly distinct from the solar neutrino mass difference. Most intriguing, the mixing angle appears to be very close to 45° – equal mixtures of two mass eigenstates.

3.3 Outlook

While a great deal of new physics has been learned from experiments on atmospheric and solar neutrinos, several important questions remain [17]:

- Oscillation experiments are sensitive to differences in the squared masses. They are not sensitive to absolute neutrino masses. We do know, from the atmospheric δm^2 , that at least

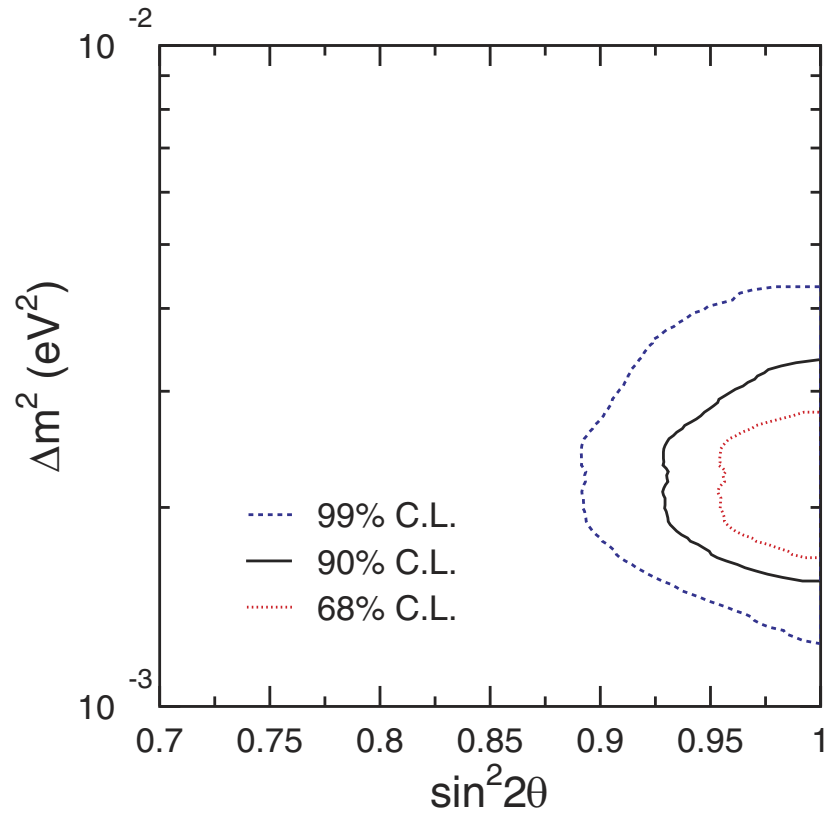


Figure 7: The Super-Kamiokande I analysis of atmospheric neutrino oscillations [16].

one neutrino must have a mass $\gtrsim 0.04$ eV. But the only laboratory bound, from tritium β decay experiments, would allow neutrino masses 50 times greater. That is, the three light neutrinos might be nearly equal in mass, split by the tiny mass differences indicated by solar and atmospheric neutrino oscillations.

- Matter effects (from passage through the Earth) have not been seen in atmospheric neutrino experiments. This leaves open two possible orderings of the mass eigenstates, as illustrated in Fig. 8.
- The solar and atmospheric mixing angles θ_{12} and θ_{23} have been determined, but a third mixing angle, θ_{13} , is so far only bounded by the results from reactor experiments, $\sin \theta_{13} \lesssim 0.17$.
- There are three CP-violating phases in the matrix that describes the relationship between neutrino mass and flavor eigenstates, one of which could be detected by looking for differences between certain conjugate oscillation channels, such as $P(\nu_e \rightarrow \nu_\mu)$ and $P(\bar{\nu}_\mu \rightarrow \bar{\nu}_e)$. Finding such a difference is important to theories that attribute the excess of matter over antimatter in our universe to leptonic CP violation.
- The neutrino, lacking an electric or any other charge that must flip sign under particle-antiparticle conjugation, is unique among standard model particles in that it may be its own antiparticle. So far no measurement has been made that can distinguish this possibility (a Majorana neutrino) from the case where the ν and $\bar{\nu}$ are distinct (a Dirac neutrino). Next-generation neutrinoless double β decay experiments

$$(N, Z) \rightarrow (N - 2, Z + 2) + 2e^-$$

could settle this issue, however. This process requires lepton number violation and Majorana masses. The two remaining CP-violating phases are Majorana phases that can affect neutrinoless double β decay rates.

- No compelling argument has been given to account for the large mixing angles deduced from atmospheric and solar neutrino oscillations. These angles differ markedly from their measured counterparts among the quarks. The special value of the atmospheric angle $\theta_{23} \sim 45^\circ$ is particularly curious.

While some of these questions may be answered in terrestrial experiments, neutrino astrophysics will continue to offer unique environments for probing fundamental neutrino properties. Several examples are given in the chapter on neutrino cooling.

4 Supernovae Neutrinos and Nucleosynthesis

The bursts associated with a core collapse supernova are among the most interesting sources of neutrinos in astrophysics [18]. A massive star, in excess of 10 solar masses, begins its lifetime burning the hydrogen in its core under the conditions of hydrostatic equilibrium. When the hydrogen is exhausted, the core contracts until the density and temperature are reached where $3\alpha \rightarrow {}^{12}\text{C}$ can take place. The helium is then burned to exhaustion. This pattern (fuel exhaustion, contraction, heating, and ignition of the ashes of the previous burning cycle) repeats several times, leading finally to the explosive burning of Si to Fe. For a heavy star, the evolution is rapid due to the

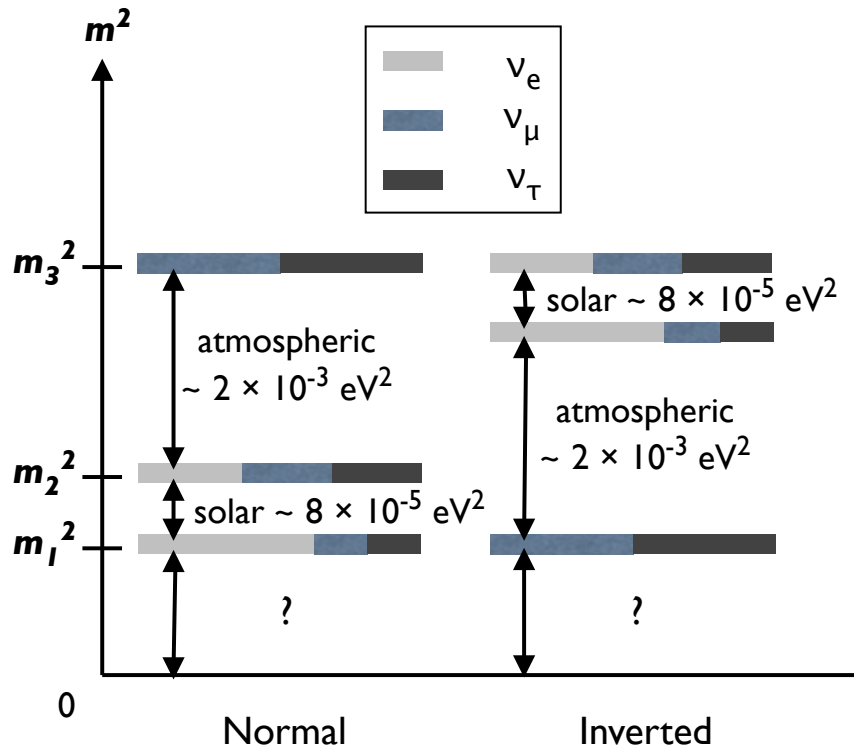


Figure 8: Illustration of the two level schemes that are possible for the light neutrinos, given that no matter effects have yet been seen in atmospheric neutrinos.

amount of energy the star must produce to support itself against its own gravity. A 25-solar-mass star would go through the set of burning cycles in about 7 My, with the final explosive Si burning stage taking a few days. The result is an “onion skin” structure of the precollapse star in which the star’s history can be read by looking at the surface inward: there are concentric shells dominated by H, ^4He , ^{12}C , ^{16}O and ^{20}Ne , ^{28}Si , and ^{56}Fe at the center.

4.1 The Explosion Mechanism and Neutrino Burst

The source of energy for this evolution is nuclear binding energy. A plot of the nuclear binding energy δ as a function of nuclear mass shows that the minimum is achieved at Fe. In a scale where the ^{12}C mass is picked as zero:

^{12}C	$\delta/\text{nucleon} = 0.000 \text{ MeV}$
^{16}O	$\delta/\text{nucleon} = -0.296 \text{ MeV}$
^{28}Si	$\delta/\text{nucleon} = -0.768 \text{ MeV}$
^{40}Ca	$\delta/\text{nucleon} = -0.871 \text{ MeV}$
^{56}Fe	$\delta/\text{nucleon} = -1.082 \text{ MeV}$
^{72}Ge	$\delta/\text{nucleon} = -1.008 \text{ MeV}$
^{98}Mo	$\delta/\text{nucleon} = -0.899 \text{ MeV}$

Once the Si burns to produce Fe, there is no further source of nuclear energy adequate to support the star. So as the last remnants of nuclear burning take place, the core is largely supported by degeneracy pressure, with the energy generation rate in the core being less than the stellar luminosity. The core density is about $2 \times 10^9 \text{ g/cc}$ and the temperature is $kT \sim 0.5 \text{ MeV}$.

Thus the collapse that begins with the end of Si burning is not halted by a new burning stage, but continues. As gravity does work on the matter, the collapse leads to a rapid heating and compression of the matter. Sufficient heating of the Fe can release α s and a few nucleons, which are bound by $\sim 8 \text{ MeV}$. At the same time, the electron chemical potential is increasing. This makes electron capture on nuclei and any free protons favorable,

$$e^- + p \rightarrow \nu_e + n.$$

As the chemical equilibrium condition is

$$\mu_e + \mu_p = \mu_n + \langle E_\nu \rangle,$$

the increase in the electron Fermi surface with density will lead to increased neutronization of the matter, as long as neutrinos freely escape the star. These escaping neutrinos carry off energy and lepton number. Both the electron capture and the nuclear excitation and disassociation take energy out of the electron gas, which is the star’s only source of support. Consequently the collapse is very rapid, with numerical simulations finding that the star’s iron core ($\sim 1.2\text{-}1.5$ solar masses) collapses at about 0.6 of the free-fall velocity.

While the ν_e s readily escape in the early stages of infall, conditions change once the density reaches $\sim 10^{12} \text{ g/cm}^3$. At this point the neutrino scattering off the matter through both charged current and coherent neutral current processes begins to alter the transport. The neutral current neutrino scattering off nuclei is particularly important, as the scattering amplitude is proportional to the total nuclear weak charge, which is approximately the neutron number. Elastic scattering transfers very little energy because the mass of the nucleus is so much greater than the typical

energy of the neutrinos. But momentum is exchanged. Because of repeated scattering the neutrino “random walks” out of the star. When the neutrino mean free path becomes sufficiently short, the time required for the neutrino to diffuse out of the high-density core begins to exceed the time scale for the collapse to be completed. Above densities of about 10^{12} g/cm³, or $\sim 1\%$ of nuclear density, such neutrino trapping occurs. Consequently, once this critical density is exceeded, the energy released by further gravitational collapse is trapped within the star until after core bounce. Similarly, the star’s lepton-number losses due to neutrino emission largely cease.

For a neutron star of 1.4 solar masses and a radius of 10 km, an estimate of its binding energy is

$$\frac{GM^2}{2R} \sim 2.5 \times 10^{53} \text{ ergs.} \quad (3)$$

Thus this is roughly the trapped energy that will later be radiated in neutrinos, after core bounce, as the proto-neutron star formed in the collapse cools.

The collapse produces a shock wave that is critical to subsequent ejection of the star’s mantle. The velocity of sound in matter rises with increasing density. Late in the collapse the sound velocity in the inner portion of the iron core, with $M_{HC} \sim 0.6 - 0.9$ solar masses, exceeds the infall velocity. Any pressure variations that may develop during infall can even out before the collapse is completed. Consequently this portion of the iron core collapses as a unit, retaining its density profile.

The collapse of the core continues until nuclear densities are reached. As nuclear matter is rather incompressible (~ 200 MeV/f³), the nuclear equation of state is effective in halting the collapse: maximum densities of 3-4 times nuclear are reached, e.g., perhaps 6×10^{14} g/cm³. The innermost shell of matter reaches this supernuclear density first, rebounds, sending a pressure wave out through the inner core. This wave travels faster than the infalling matter, as the inner iron core is characterized by a sound speed in excess of the infall speed. Subsequent shells follow. The resulting pressure waves collect at the edge of the inner iron core – the radius at which the infall velocity and sound speed are equal. As this point reaches nuclear density and comes to rest, a shock wave breaks out and begins its traversal of the outer core.

Initially the shock wave may carry an order of magnitude more energy than is needed to eject the mantle of the star (less than 10^{51} ergs). But as the shock wave travels through the outer iron core, it heats and melts the iron that crosses the shock front, at a loss of ~ 8 MeV/nucleon. Additional energy is lost by neutrino emission, which increases after the melting. These losses are comparable to the initial energy carried by the shock wave. Most simplified (e.g., one dimensional) numerical models fail to produce a successful “prompt” hydrodynamic explosion, for this reason. The shock stalls near the edge of the iron core, instead of propagating into the mantle.

Most of the theoretical attention in the past decade has focused on the role of neutrinos in reviving this shock wave, a process that becomes more effective in multi-dimensional models that account for convection. In this delayed mechanism, the shock wave stalls at a radius of 200-300 km, some tens of milliseconds after core bounce. But neutrinos diffusing out of the proto-neutron star react frequently in the nucleon gas left in the wake of the shock wave, depositing significant energy. Over ~ 0.5 seconds the increasing pressure due to neutrino heating of this nucleon gas helps push the shock outward. This description is over-simplified – a variety of contributing effects are emerging from numerical simulations – but there is wide agreement that energy deposition by neutrinos is an essential ingredient for successful explosions.

Regardless of explosion details, neutrinos dominate supernova energetics. The kinetic energy of the explosion and supernova’s optical display account for less than 1% of the available energy.

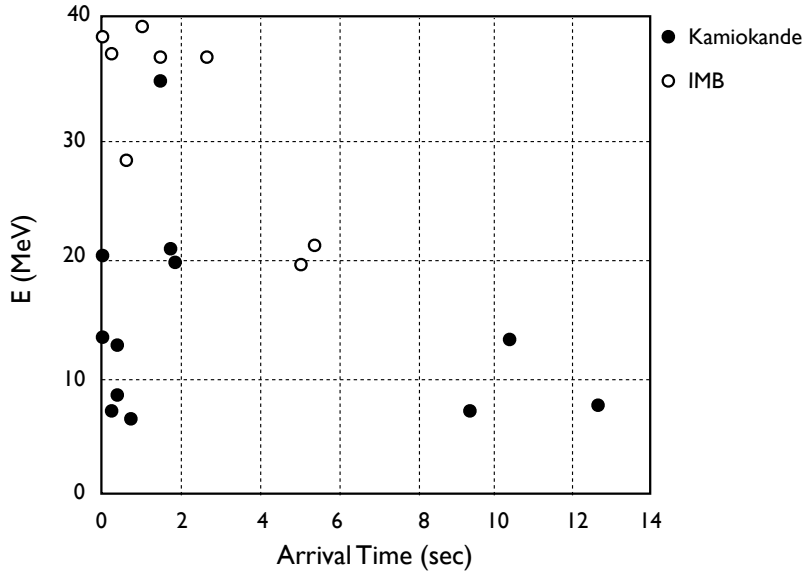


Figure 9: The timing and energy of neutrino events from SN1987A, as observed in the Kamiokande and IMB detectors [19].

The remaining 99% of the 3×10^{53} ergs released in the collapse is radiated in neutrinos of all flavors. The timescale over which the trapped neutrinos leak out of the proto-neutron star is about three seconds. The energy is roughly equipartitioned among the flavors (a consequence of reactions among trapped neutrinos that equilibrate flavor). The detailed decoupling of the emitted neutrinos from the matter – which occurs at a density of about $10^{11} - 10^{12}$ g/cm³ – does depend on flavor. This leads to differences in neutrino temperatures, with electron neutrinos being somewhat cooler ($T \sim 3.5$ MeV) than the heavy-flavor neutrinos ($T \sim 6$ MeV). The radius for neutrino-matter decoupling defines a “neutrinosphere” deep within the star, analogous to the familiar photosphere for optical emissions.

The burst of neutrinos produced in a galactic core-collapse supernova is detectable with instruments like Super-Kamiokande and SNO. On February 23, 1987, a neutrino burst from a supernova in the Large Magellanic Cloud was observed in the proton-decay detectors Kamiokande and IMB [19]. The optical counterpart reached an apparent magnitude of about 3, and could be observed easily in the night sky with the naked eye. This supernova originated 160,000 light years from Earth. Approximately 20 events were seen in the Kamiokande and IBM detectors, spread over approximately 10 seconds. Within the limited statistics possible with these first-generation detectors, the number of events and the burst duration were consistent with standard estimates of the energy release and cooling time of a supernova. The neutrino data from the two detectors are shown in Fig. 9.

Temperature differences between neutrino flavors are interesting because of oscillations and nucleosynthesis. The discussion of matter effects in the solar neutrino problem was limited to two

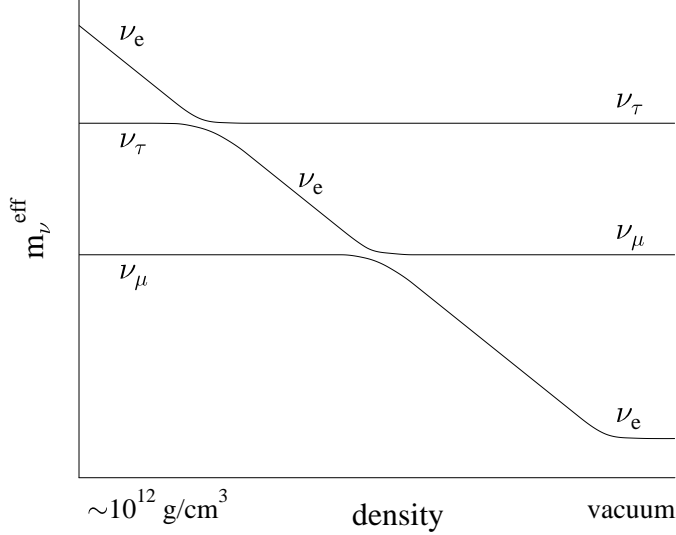


Figure 10: A schematic illustration of the two level crossings that the ν_e would experience, given the higher densities available in the mantle of a massive star undergoing core collapse.

flavors. But the higher densities found in core-collapse supernovae make all three flavors relevant. The three-flavor MSW level-crossing diagram is shown in Fig. 10. One sees, in addition to the neutrino “level crossing” $\nu_\mu \leftrightarrow \nu_e$ important for solar neutrinos, a second crossing of the ν_e with the ν_τ . The higher density characterizing this second crossing, $\sim 10^4 \text{ g/cm}^3$, is determined by atmospheric mass difference δm_{23}^2 and by the typical energy of supernova neutrinos, $\sim 10 - 20 \text{ MeV}$. This density is beyond that available in the Sun ($\lesssim 10^2 \text{ g/cm}^3$), but far less than that of a supernova’s neutrinosphere. Consequently this second level crossing alters neutrino flavor only after the supernova neutrinos are free-streaming out of the star, with well defined spectra that are approximately thermal. This level crossing can exchange the flavor labels on the ν_e and ν_τ spectra, so that the ν_e s become hotter than the heavy-flavor neutrinos. One would expect such an inversion to be apparent in terrestrial supernova neutrino detectors.

In fact this description oversimplifies the neutrino physics of supernovae. The enormous neutrino densities encountered in a supernova lead to a new aspect of the MSW effect – oscillations altered not by neutrino-electron scattering, but by neutrino-neutrino scattering [20]. While the precise consequences of this neutrino-neutrino MSW potential are still being debated, the effects reach much deeper into the star and alter the flavor physics in distinctive ways. Supernovae likely provide the only environment in nature where neutrino-neutrino interactions dominate the MSW potential.

4.2 Supernova Neutrino Physics

This novel neutrino-neutrino MSW potential is one of many reasons core-collapse supernovae play an important role in neutrino astrophysics. Others include:

- The second level crossing involves the third, as yet unmeasured mixing angle θ_{13} . This level-crossing occurs in the star’s mantle and remains adiabatic – the condition for flavor inversion – for mixing angles $\sin^2 2\theta_{13} \gtrsim 10^{-4}$. This kind of sensitivity to small mixing angles is not achievable in the next generation of terrestrial neutrino experiments, which have goals of $\gtrsim 10^{-2}$. Thus supernovae may provide our only near-term hope of constraining this mixing angle, should it prove small.
- Neutrinos from galactic supernovae will not be obscured by intervening matter or dust, unlike optical signals. Thus supernova neutrino bursts should, over the next few hundred years, provide our most reliable measure of the contemporary rate of galactic core collapse.
- There exists a so-far undetected diffuse background of supernova neutrinos, produced by all past supernovae occurring in the universe. Future detectors that may approach the megaton scale should be able to see a few events from this source. Detection of these neutrinos would place a important constraint on the inventory of massive stars undergoing core collapse, from the first epoch of star formation until now.
- Supernovae are one of the most important engines for nucleosynthesis, controlling much of the chemical enrichment of the galaxy. As described in the next section, neutrinos are directly and indirectly involved in this synthesis.
- While most of the energy released in core collapse is radiated as neutrinos over the first several seconds, neutrino emission at a lower level continues as the proto-neutron star cools and radiates away its lepton number. It is quite possible that phase changes in the dense nuclear matter could occur several tens of seconds after core bounce, altering the late-time neutrino “light curve” in a characteristic way. While there are considerable uncertainties in estimates, neutrino processes may continue to dominate neutron star cooling for $\sim 10^5$ years.
- The neutrino burst could include other sharp features in time, marking interesting astrophysics. The melting of iron to nucleons with the passage of the shock wave through the outer iron core is predicted to produce a spike in the neutrino luminosity, lasting for a few milliseconds. Continued accretion onto the neutron star surface could produce a collapse to a black hole, and consequently a sudden termination in neutrino emission.
- Supernova cooling times place constraints on new physics associated with particles that also couple weakly to matter. For example, a light scalar called the axion could, in principle, compete with neutrinos in cooling a supernovae. The requirement that axion emission not shorting the cooling time too much, which would be in conflict with SN1987A data, constrains the mass and coupling of this hypothesized particle.

5 Neutrinos and Nucleosynthesis

Neutrinos and nucleosynthesis are both associated with explosive environments found in astrophysics. This section discusses three examples, the Big Bang, the neutrino process, and the r-process.

5.1 Neutrinos in Big-Bang Nucleosynthesis (BBN)

One of the classic problems in nucleosynthesis and cosmology is accounting for the mass fraction of primordial helium of 25%, as well as the abundances of D, ^3He , and ^7Li . The ^4He mass fraction shows that nuclei were synthesized from the early-universe nucleon soup at a time when the n/p ratio was $\sim 1/7$. This requires the proper coordination of two “clocks,” one being the weak interaction rate for decay of free neutrons to protons, and the other the Hubble rate governing the expansion of the universe,

$$H(t) \equiv \frac{1}{R(t)} \frac{dR(t)}{dt} = \sqrt{\frac{8\pi G \rho(t)}{3}},$$

where G is the gravitational constant. This clock depends on the energy density $\rho(t)$ which, at this epoch, is dominated by relativistic particles, including the neutrinos. BBN also includes one adjustable parameter, the baryon density, which is usually given in terms of the ratio of baryons to photons η . But the primordial abundance of ^4He is relatively insensitive to η , in contrast to other BBN species like D. Furthermore an independent and quite precise determination of η has now been derived from the pattern of acoustic peaks seen in mappings of the cosmic microwave background. Consequently the abundance of ^4He is a rather good test of the number of neutrino flavors contributing to early-universe expansion.

Detail analyses find that a consistent picture emerges. The number of neutrino species is found to be $N_\nu = 2.4 \pm 0.4$. One can adopt the expected value of $N_\nu = 3$ and reproduce the abundances of both D and ^4He at the 68% confidence level [21].

This standard use of BBN is now mostly of historical interest, though at one time it was the best test of the number of light neutrino species. However, there are variations of the BBN analysis that are of significant current interest, such as the consequences of a net lepton number asymmetry in the universe, or the presence of a sterile neutrino (a neutrino lacking standard-model couplings) that might mix with active species. Such phenomena affect resulting abundances, and thus can be constrained in a BBN analysis.

5.2 The Neutrino Process

One of the more amusing roles for neutrinos in nucleosynthesis is found in the neutrino process, the direct synthesis of new elements through neutrino reactions. Core-collapse supernovae provide the enormous neutrino fluences necessary for such synthesis to be significant. They also eject newly synthesized material into the interstellar medium, where it can be incorporated into a new generation of stars.

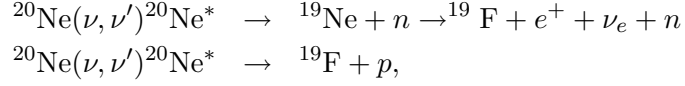
Among the elements that might be made primarily or partially in the ν -process, the synthesis of ^{19}F is one of the more interesting examples [22]. The only stable isotope of fluorine, ^{19}F has an abundance

$$\frac{^{19}\text{F}}{^{20}\text{Ne}} \sim \frac{1}{3100}.$$

Ne is one of the hydrostatic burning products in massive stars, produced in great abundance and ejected in core-collapse supernovae. Thus a mechanism that converts $\sim 0.03\%$ of the ^{20}Ne in the star’s mantle into ^{19}F could account for the entire observed abundance of the latter.

The Ne zone in a supernova progenitor star is typically located at a radius of $\sim 20,000$ km. A simple calculation that combines the neutrino fluence through the Ne zone with the cross section for inelastic neutrino scattering off ^{20}Ne shows that approximately 0.3% of the ^{20}Ne nuclei would

interact with the neutrinos produced in the core collapse. Almost all of these reactions result in the production of ^{19}F , e.g.,



with the first reaction occurring half as frequently as the second. Thus one would expect the abundance ratio to be $^{19}\text{F}/^{20}\text{Ne} \sim 1/300$, corresponding to an order of magnitude more ^{19}F than found in nature.

This example shows that stars are rather complicated factories for nucleosynthesis. Implicit in the reactions above are mechanisms that also destroy ^{19}F . For example, about 70% of the neutrons coproduced with ^{19}F in the first reaction immediately recapture on ^{19}F , destroying the product of interest. Similarly, many of the coproduced protons destroy ^{19}F via $^{19}\text{F}(p, \alpha)^{16}\text{O}$ – unless the star is rich in ^{23}Na , which readily consumes protons via $^{23}\text{Na}(p, \alpha)^{20}\text{Ne}$. Finally, some of the ^{19}F produced in the neon shell is destroyed when the shock wave passes through that zone: the shock wave can heat the inner portion of the Ne zone above $1.7 \times 10^9\text{K}$, the temperature at which ^{19}F can be destroyed by $^{19}\text{F}(\gamma, \alpha)^{15}\text{N}$.

If all of this physics is treated carefully in a nuclear network code, one finds that the desired $^{19}\text{F}/^{20}\text{Ne} \sim 1/3100$ is achieved for a heavy-flavor neutrino temperature of about 6 MeV. This is quite consistent with the temperatures that come from supernova models.

The neutrino process produces interesting abundances of several relatively rare, odd- A nuclei including ^7Li , ^{11}B , ^{138}La , ^{180}Ta , and ^{15}N . Charged-current neutrino reactions on free protons can produce neutrons that, through (n, p) and (n, γ) reactions, lead to the nucleosynthesis of the so-called “p-process” nuclei from $A=92$ to 126. The production of such nuclei has been a long-standing puzzle in nuclear astrophysics.

5.3 The r-process

Beyond the iron peak nuclear Coulomb barriers become so high that charged particle reactions become ineffective, leaving neutron capture as the mechanism responsible for producing the heaviest nuclei. If the neutron abundance is modest, this capture occurs in such a way that each newly synthesized nucleus has the opportunity to β decay, if it is energetically favorable to do so. Thus weak equilibrium is maintained within the nucleus, so that synthesis is along the path of stable nuclei. This is called the s- or slow-process. However a plot of the s-process in the (N, Z) plane reveals that this path misses many stable, neutron-rich nuclei that are known to exist in nature. This suggests that another mechanism is at work, too. Furthermore, the abundance peaks found in nature near masses $A \sim 130$ and $A \sim 190$, which mark the closed neutron shells where neutron capture rates and β decay rates are slower, each split into two subpeaks. One set of subpeaks corresponds to the closed-neutron-shell numbers $N \sim 82$ and $N \sim 126$, and is clearly associated with the s-process. The other set is shifted to smaller $N \sim 76$ and ~ 116 , respectively, suggestive of a much more explosive neutron capture environment.

This second process is the r- or rapid-process [23], which requires a neutron fluence so large that neutron capture is fast compared to β decay. In this case nuclei rapidly absorb neutrons until they approach the neutron drip line. That is, equilibrium is maintained by $(n, \gamma) \leftrightarrow (\gamma, n)$, not by weak interactions. Consequently the nuclei participating in the r-process are very different from ordinary nuclei – very neutron rich nuclei that would decay immediately in the low-temperature environment

of Earth. The rate of nucleosynthesis is controlled by the rate of β decay: a new neutron can be captured only after β decay, $n \rightarrow p + e^- + \bar{\nu}_e$, opens up a hole in the neutron Fermi sea. Consequently one expects abundance peaks near the closed neutron shells at $N \sim 82$ and 126 , as β decay is slow and mass will pile up at these “waiting points.” By a series of rapid neutron captures and slower β decays, synthesis can proceed all the way to the transuranics. This, of course, requires the very explosive conditions necessary to support large neutron densities (typically $\rho(n) \sim 10^{18} - 10^{20}/\text{cm}^3$, temperatures $\sim 10^9$ K), sufficient time (~ 1 second), and a ratio of neutrons to heavy seed nuclei of $\gtrsim 100$ (so that there are enough neutrons to add to each seed nucleus).

The path of the r-process is along neutron-rich nuclei, where the neutron Fermi sea is just $\sim (2-3)$ MeV away from the neutron drip line (where no more bound neutron levels exist). After the r-process finishes (the neutron exposure ends) the nuclei decay back to the valley of stability by β decay. This involves conversion of neutrons into protons, and that shifts the r-process peaks from the parent-nucleus values of $N \sim 82$ and 126 to lower values for the stable daughter nuclei, off course. This effect is clearly seen in the abundance distribution – a very strong hint that many familiar heavy nuclei came from parents created in exotic, explosive environments.

The role of neutrinos in the r-process is in maintaining that explosive, neutron-rich environment: while there are alternatives, perhaps the most plausible site is the neutrino-driven wind – the last ejecta blown off the neutron star – of core-collapse supernovae. This material is a hot, radiation-dominated gas containing neutrons and protons, with an excess of neutrons. As the nucleon gas expands off the star and cools, it goes through a freezeout to α particles, a step that essentially locks up all the protons in this way. Then the α s interact through reactions like

$$\alpha + \alpha + \alpha \rightarrow {}^{12}\text{C}$$

to start forming heavier nuclei. The α capture continues, eventually synthesizing intermediate-mass “seed” nuclei. Once these seed nuclei are produced, if the requisite number of neutrons is available (~ 100 per seed nucleus) the synthesis of very heavy nuclei is possible. The scenario, as depicted in Fig. 11, is quite similar to the Big Bang: a hot nucleon gas (with an entropy $S \sim 100$ in Boltzmann units, compared to the BBN $S \sim 10^{10}$) expand and cools, condensing into nuclei. But a detail – the neutrino wind has an excess of neutrons, while the Big Bang is proton-rich – leads to the synthesis of uranium in one case, and to termination of nucleosynthesis at ${}^4\text{He}$ (plus a few light elements) in the other. Some of the supernova modelers find conditions where a neutrino-wind r-process almost happens. The neutrinos are crucial: they help keep the entropy of the nucleon gas high, control the n/p ratio of the gas through competing charge-current reactions, and generate the wind that ejects the r-process products.

There are some very nice aspects of this site: the amount of matter ejected is $\sim 10^{-5} - 10^{-6}$ solar masses, a production per event that if integrated over the lifetime of the galaxy gives the required total abundance of r-process metals, assuming typical supernova rates. There are also a few problems, especially the fact that with calculated entropies, the neutron fractions in the nucleon soup above the proto-neutron star appear too low to produce a successful $A \sim 190$ peak. This may reflect our incomplete understanding of the supernova mechanism, or possibly our inability to model the weak interactions (including the effects of neutrino oscillations) adequately.

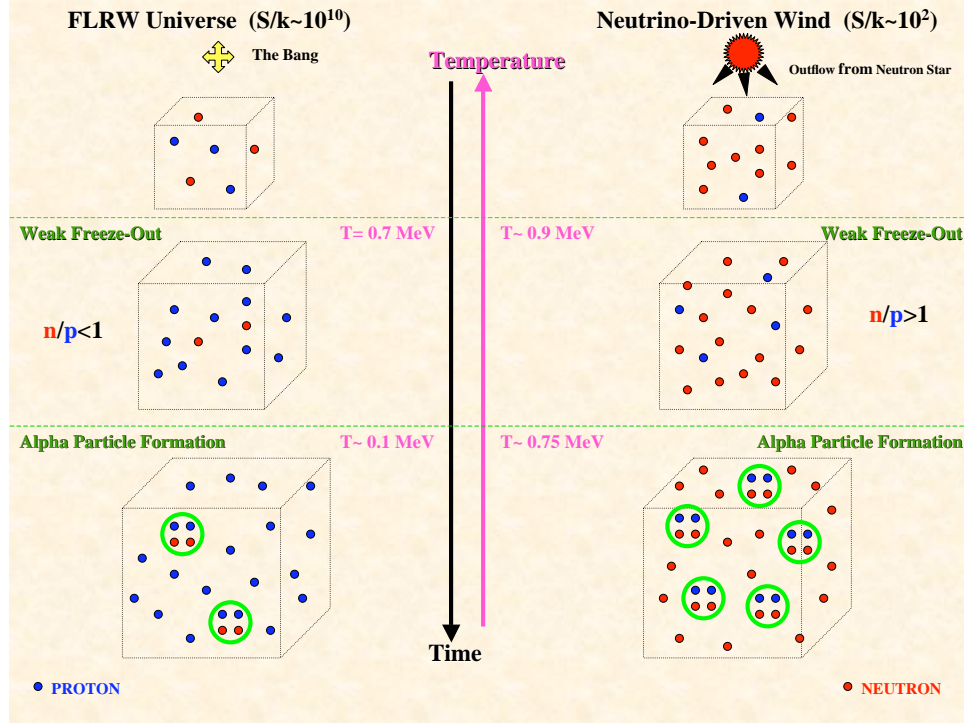


Figure 11: A comparison of two remarkably similar mechanisms for nucleosynthesis, an expanding, cooling, high entropy, proton-rich nucleon gas (the Big Bang, left panel) and an expanding, cooling, high entropy, neutron-rich nucleon gas (the supernova wind r-process, right panel). In the former, the synthesis determinates at ^4He and a few other light elements. In the latter, the synthesis continues to the heavy transuranic elements. Figure from G. Fuller.

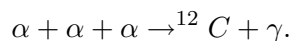
6 Neutrino Cooling and Red Giants

Several neutrino cooling scenarios have already been discussed, including cooling of the proto-neutron star produced in core collapse and cooling connected with the expansion of the early universe. Red giant cooling provides an additional example of the use of astrophysical arguments to constrain fundamental properties of neutrinos.

6.1 Red Giants and Helium Ignition

In a solar-like star, when the hydrogen in the central core has been exhausted, an interesting evolution ensues:

- With no further means of producing energy, the core slowly contracts, thereby increasing in temperature as gravity does work on the core.
- Matter outside the core is still hydrogen rich, and can generate energy through hydrogen burning. Thus a hydrogen-burning shell forms, generating the gas pressure supporting the outside layers of the star. As the ${}^4\text{He}$ -rich core contracts, the matter outside the core is also pulled deeper into the gravitational potential. Furthermore, the H-burning shell continually adds more mass to the core. This means the burning in the shell must intensify to generate the additional gas pressure to fight gravity. The shell also thickens, as more hydrogen is above the burning temperature.
- The resulting increasing gas pressure causes the outer envelope of the star to expand by a large factor, up to a factor of 50. The increase in radius more than compensates for the increased internal energy generation, so that a cooler surface results. The star reddens. Stars of this type are called red supergiants.
- This evolution is relatively rapid, perhaps a few hundred million years: the dense core requires large energy production. The helium core is supported by its degeneracy pressure, and is characterized by densities $\sim 10^6 \text{ g/cm}^3$. This stage ends when the core reaches densities and temperatures that allow helium burning through the reaction



As this reaction is quite temperature dependent, the conditions for ignition are very sharply defined. This has the consequence that the core mass at the helium flash point is well determined.

- The onset of helium burning produces a new source of support for the core. The energy released elevates the temperature and the core expands: He burning, not electron degeneracy, now supports the core. The burning shell and envelope move outward, higher in the gravitational potential. Thus shell hydrogen burning slows (the shell cools) because less gas pressure is needed to satisfy hydrostatic equilibrium. All of this means the evolution of the star has now slowed: the red giant moves along the “horizontal branch,” as interior temperatures increase slowly, much as in the main sequence.

The 3α process involves some fascinating nuclear physics that will not be recounted here: the existence of certain nuclear resonances was predicted based on the astrophysical requirements for

this process. The resulting He-burning rate exhibits a sharp temperature dependence $\sim T^{40}$ in the range relevant to red giant cores. This dependence is the reason the He flash is delicately dependent on conditions in the core.

6.2 Neutrino Magnetic Moments and He Ignition

Prior to the helium flash, the degenerate He core radiates energy largely by neutrino pair emission. The process is the decay of a plasmon — which one can think of as a photon “dressed” by electron-hole excitations — thereby acquiring an effective mass of about 10 keV. The photon couples to an electron particle-hole pair that then decays via $Z_o \rightarrow \nu\bar{\nu}$.

If this cooling is somehow enhanced, the degenerate helium core would not ignite at the normal time, but instead continue to grow. When the core does finally ignite, the larger core will alter the star’s subsequent evolution.

One possible mechanism for enhanced cooling is a neutrino magnetic moment. Then the plasmon could directly couple to a neutrino pair. The strength of this coupling would depend on the size of the magnetic moment.

A delay in the time of He ignition has several observable consequences, including changing the ratio of red giant to horizontal branch stars. Thus, using the standard theory of red giant evolution, investigators have attempted to determine what size of magnetic moment would produce unacceptable changes in the astronomy. The result is a limit [24] on the neutrino magnetic moment of

$$\mu_{ij} \lesssim 3 \times 10^{-12} \text{ electron Bohr magnetons.}$$

This limit is two orders of magnitude more stringent than that obtained from direct laboratory tests, e.g., experiments looking for the effect of a neutrino magnetic moment in the scattering of reactor neutrinos off electrons.

This example is just one of a number of such constraints that can be extracted from similar stellar cooling arguments. The arguments above, for example, can be repeated for neutrino electric dipole moments, or for axion emission from red giants. As noted previously, the arguments can be extended to supernovae: anomalous cooling processes that shorten the cooling time in a way that is inconsistent with SN1987A observations are ruled out. Limits can also be placed on Dirac neutrino masses: the mass term would allow neutrinos to scatter into sterile right-handed states, which would then immediately escape, carrying off energy.

7 High Energy Astrophysical Neutrinos

The previous discussion focused on astrophysical neutrino sources with energies ranging from the cosmic microwave/neutrino temperature to $\lesssim 10$ GeV, which includes the bulk of atmospheric neutrinos. These sources are displayed in Fig. 12 according to their contributions to the terrestrial flux density. This figure includes sources, such as the thermal solar neutrinos of all flavors, not explicitly discussed here because of space limitations. However, the spectrum of neutrinos is believed to extend to far higher energies due to neutrino production in some of nature’s most spectacular natural accelerators. The program of experiments to map out the high-energy neutrino spectrum and its astrophysical sources is just beginning. Some guidance is provided by existing data on cosmic-ray protons, nuclei, and γ rays, which constrain possible neutrino fluxes (see Fig. 13). This

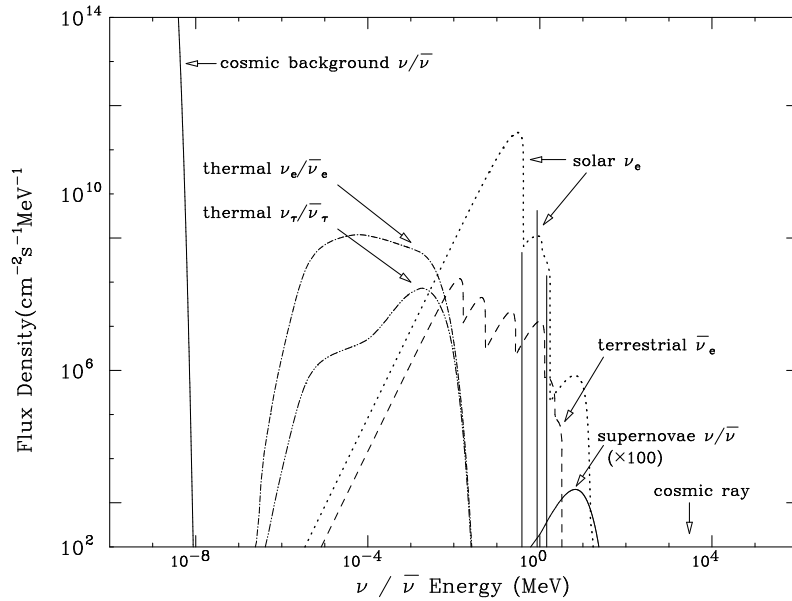


Figure 12: The low-energy neutrino “sky.” In addition to the principal sources discussed in the text (Big-Bang, solar, supernova, and atmospheric neutrinos), the natural neutrino background includes ~ 1 keV thermal neutrinos of all flavors emitted by the sun as well as $\bar{\nu}_e$ s generated by the Earth’s natural radioactivity. From [25].

concluding chapter discusses some of the suggested sources and current efforts to develop high-energy neutrino telescopes appropriate to these sources. The high-energy spectrum is one of the frontiers of neutrino astronomy.

7.1 Neutrino Production by Cosmic Rays

The ultra-high-energy cosmic ray (UHECR) spectrum – presumably protons and nuclei – is known to vary smoothly up to an energy $E \sim 4 \times 10^{19}$ eV. The spectrum just below this point is characterized by a spectral index $\alpha \sim -2.7$: the flux varies as E^α [27]. Higher energy events are seen, but the flux drops off steeply beyond this point. This is consistent with the prediction of Greisen, Zatsepin, and Kuz’mín [28] of a cutoff in the spectrum above $\sim 4 \times 10^{19}$ eV. Above this cutoff UHECRs can lose energy by scattering off microwave photons, producing pions. This sharply reduces the mean-free path of such UHECRs. The flux drops, reflecting the reduced number of sources within a mean-free path of the Earth.

An estimate can be made of the flux of UHE neutrinos associated with the decays of pions and other secondaries produced in the GZK scattering. Uncertainties in this estimate include the flux, spectrum, and composition of the UHECRs, the behavior of the spectrum beyond the GZK cutoff (as we are blind to these UHECRs), and the spectrum’s cosmological evolution. One bound was obtained by Bahcall and Waxman [29]; another is shown in Fig. 13.

These uncertainties are connected to some very interesting astrophysical issues: the maximum

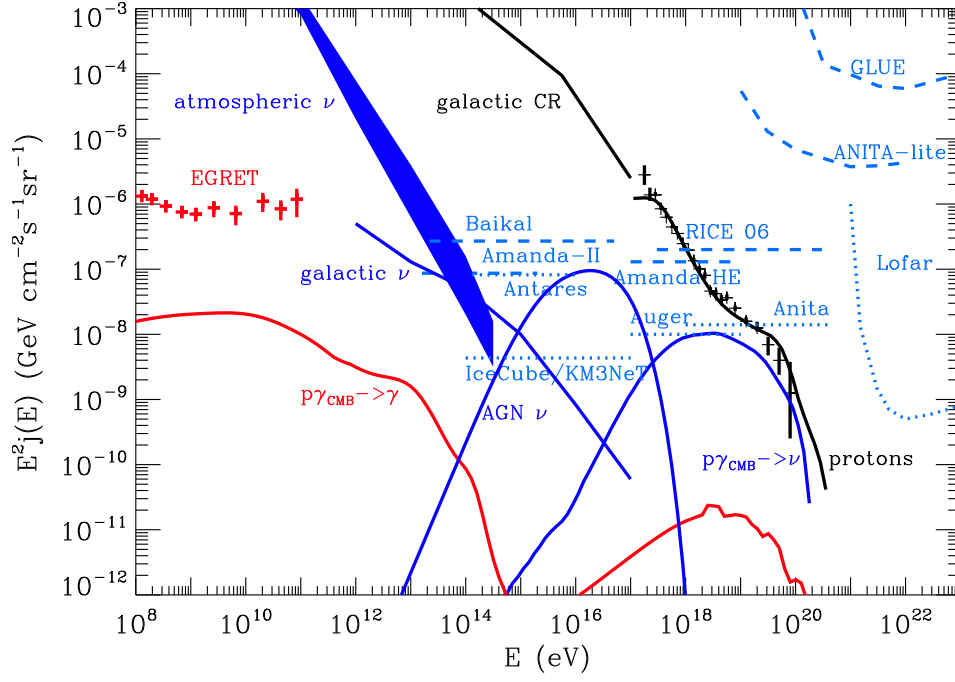


Figure 13: A theoretical model of high-energy neutrino “sky.” Shown are the expected neutrino fluxes (blue area and lines), the primary cosmic ray fluxes (determined from data and a model, black), and the secondary γ -ray fluxes expected from protons interacting with the microwave background (red). The neutrino flux is per flavor and includes only relatively certain sources: atmospheric neutrinos, neutrinos resulting from cosmic-ray interactions in our galaxy, and GZK neutrinos resulting from cosmic-ray interactions with the microwave and infrared background. The figure includes experimental data, limits, and projected sensitivities to existing and planned telescopes. Figure from G. Sigl [26].

energies that can be reached in astrophysical accelerators; the UHECR uniformity over time (or equivalently redshift); and the role other background photon sources, such as the infrared and optical backgrounds, in producing UHE neutrinos. A more extended assumption can be found in [17].

As in the case of low-energy sources such as solar neutrinos, the detection of very high energy astrophysical neutrinos would open up new opportunities in both astrophysics and particle physics. Because the GZK cutoff limits the range of the UHECRs, neutrinos provide the only direct probe of nature’s most energetic astrophysical accelerators. Because neutrinos travel in straight lines through magnetic fields, they point back to their sources, allowing astronomers to correlate those sources with their optical counterparts – the accretion disks surrounding supermassive black holes, quasars, γ -ray bursts, etc. The interactions of such energetic neutrinos with matter are untested experimentally, as terrestrial accelerators have reach only the TeV scale.

7.2 Point Sources and Neutrino Telescopes

The possibility of point sources is generally considered the astrophysical “driver” for developing instruments to measure the highest energy neutrinos. There are intensely energetic sources in the sky, including active galactic nuclei (AGNs), supernovae and phenomena like γ -ray bursts that may be associated with particularly energetic supernovae, and compact objects such as black holes and neutron stars. The magnetic fields, shock waves, gravitational fields, and energy densities associated with such objects are beyond those that can be produced in the laboratory.

There are recent results that further motivate such neutrino studies. The cosmic-ray telescope Pierre Auger (see Fig. 14), in its studies of events near the GZK cutoff, has found correlations between clusters of events and nearby AGNs: At these energies the trajectories of protons and nuclei are not strongly perturbed by magnetic fields, so that these also point back to their sources [27]. Once one can attribute events to an astrophysical source, then those events become a probe of that object. In this particular case, one is then challenged to explain the mechanism by which an AGN accelerates nucleons or nuclei to, and perhaps beyond, $\sim 10^{20}$ eV. Were neutrinos also seen, the relative yields of high-energy nuclei and neutrinos would place important constraints on the astrophysical accelerator. Similarly, γ -ray bursts, the most luminous electromagnetic events found in the universe, appear to be highly beamed emissions of a few seconds in duration. A few such events are detected each week. One popular model associates these emissions with jets produced in the collapse of the core of a very massive star into a black hole. Detection (or failure to detect) neutrinos from such a source could help modelers determine whether the plasmas accelerated by such jets contain a significant density of nucleons and nuclei, as photonuclear excitation would necessarily lead to neutrinos.

The challenge in the field of UHE neutrinos is to build telescopes with the necessary sensitivity to see events, given current estimates of the fluxes (see Fig. 13). This requires instrumenting very large volumes. There have been ongoing efforts to use large quantities of water and ice as detectors, with experiments developed or planned in lakes (Baikal), in the Antarctic (AMANDA), and in oceans (NESTOR, ANTARES) [17]. IceCube [30], a project that will extend the dimensions of such detectors to a cubic kilometer, is now under construction at the South Pole (Fig. 15). This telescope, when completed, will view the ice through approximately 4200 optical modules, deployed on 70 vertical strings at a depth of 1450 to 2450m. At this depth the clarity of the ice enhances event detection. This deep detector is coupled to a surface air-shower array. Approximately half of the strings have been deployed; the completion of the entire array is expected by 2011.

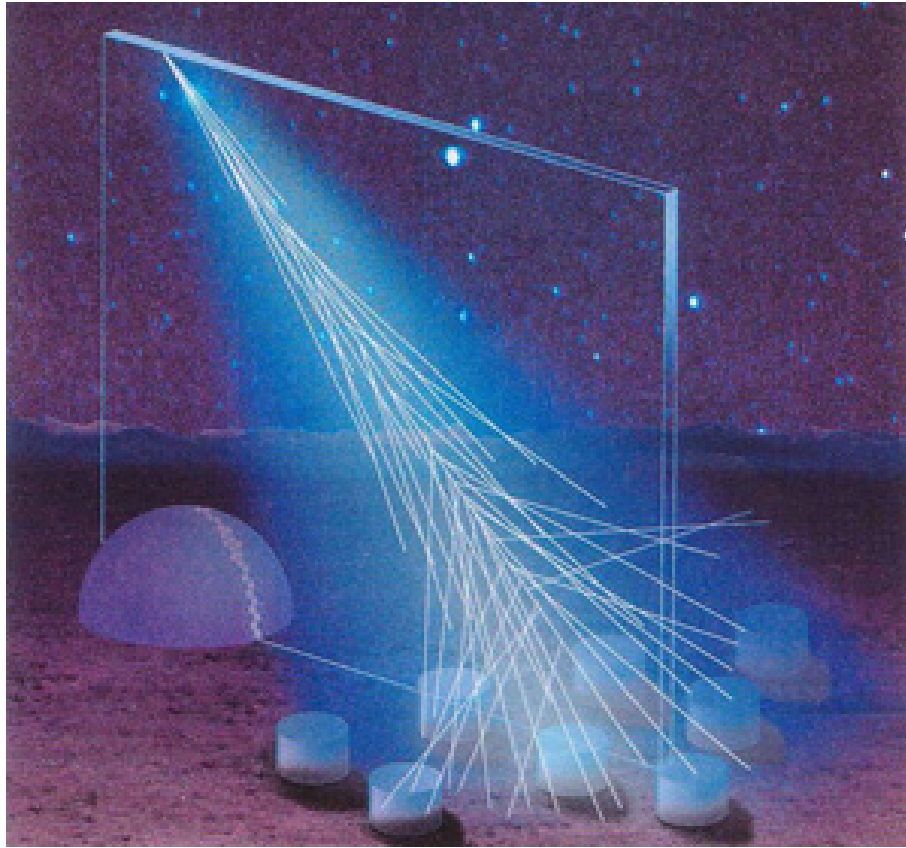


Figure 14: A conceptual drawing of the Pierre Auger cosmic ray observatory, which combines an array of surface detectors (tanks containing water) with air-florescence telescopes (which track the development of air showers through the ultraviolet light they produce) to better determine the energy of UHECRs. Figure coutesy of the Pierre Auger Observatory.

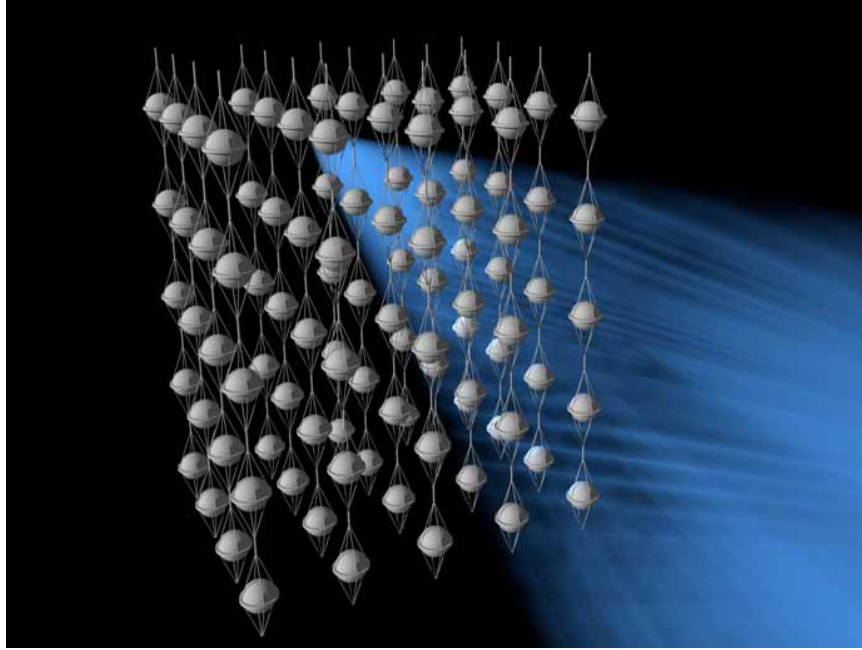


Figure 15: Artist's rendering of the IceCube detector, showing the optical modules arrayed on strings within the deep ice and a cone of blue Cerenkov light produced by a neutrino scattering within the detector. Figure courtesy of the IceCube Project, University of Wisconsin, Madison [30].

8 Acknowledgement

This work was supported in part by the U.S. Department of Energy, Office of Nuclear Physics, under grant #DE-FG02-00ER41132.

References

- [1] W. C. Haxton and B. R. Holstein, Am. J. Phys. **68** (2000) 15 and **72** (2004) 18.
- [2] J. N. Bahcall, *Neutrino Astrophysics*, (Cambridge University, Cambridge, 1989).
- [3] R. Davis Jr., D. S. Harmer, and K. C. Hoffman, Phys. Rev. Lett. **20** (1966) 1205.
- [4] J. N. Bahcall, A. Serenelli, and S. Basu, Ap. J. **621** (2005) L85.
- [5] A. S. Brun, S. Turck-Chieze, and P. Morel, Ap. J. **506** (1998) 913.
- [6] J. N. Bahcall and M. H. Pinsonneault, Phys. Rev. Lett. **92** (2004) 121301.
- [7] J. Hosaka *et al.*, Phys. Rev. **D73** (2006) 112001; J. P. Cravens *et al.*, arXiv:0803.4312 (2008).
- [8] Q. R. Ahmad *et al.*, Phys. Rev. Lett. **89** (2002) 011301.
- [9] Q. R. Ahmad *et al.*, Phys. Rev. **C75** (2007) 045502.
- [10] S. P. Mikheyev and A. Smirnov, Sov. J. Nucl. Phys. **42** (1985) 913.
- [11] L. Wolfenstein, Phys. Rev. **D17** (1979) 2369.
- [12] B. Aharmim *et al.*, arXiv:0806.0989 (submitted to Phys. Rev. Lett.); KamLAND Collaboration, Phys. Rev. Lett. **92** (2005) 081801.
- [13] Borexino Collaboration, Phys. Lett. **B658** (2008) 101.
- [14] T. J. Haines *et al.*, Phys. Rev. Lett. **20** (1986) 1986; D. Casper *et al.*, Phys. Rev. Lett. **66** (1991) 2561.
- [15] K. S. Hirata *et al.*, Phys. Lett. **B205** (1988) 416.
- [16] Y. Fukuda *et al.*, Phys. Rev. Lett. **81** (1998) 1562.
- [17] *APS Mult-Divisional Study of the Physics of Neutrinos*, <http://www.aps.org/policy/reports/multidivisional/neutrino/>.
- [18] H.-Th. Janka, K. Langanke, A. Marek, G. Martinez-Pinedo, and B. Muller, Phys. Rep. **442** (2007) 38; A. Mezzacappa, Ann. Rev. Nucl. Part. Sci. **55** (2005) 467; K. Kotake, K. Sato, and K. Takahashi, Rep. Prog. Phys. **69** (2006) 971; S. Woosley and J. S. Bloom, Ann. Rev. Astron. Astrophys. **44** (2006) 507.
- [19] K. Hirata *et al.*, Phys. Rev. Lett. **58** (1987) 1490; R. M. Bionta *et al.*, Phys. Rev. Lett. **58** (1987) 1494.

- [20] G. M. Fuller, R. W. Mayle, J. R. Wilson, and D. N. Schramm, *Ap. J.* **322** (1987) 795; D. Notzold and G. Raffelt, *Nucl. Phys.* **B307** (1988) 924.
- [21] G. Steigman, *Ann. Rev. Nucl. and Part. Sci.* **57** (2007) 463.
- [22] S. E. Woosley, D. H. Hartmann, R. D. Hoffman, and W. C. Haxton, *Ap. J.* **356** (1990) 272.
- [23] Y.-Z. Qian, *Prog. Part. Nucl. Phys.* **50** (2003) 153.
- [24] G. G. Raffelt, *Phys. Rev. Lett.* **64** (1990) 2856.
- [25] W.C. Haxton and W. Lin, *Phys. Lett.* **B486** (2000) 263.
- [26] G. Sigl, *Nuc. Phys. Proc. Suppl.* **168** (2007) 219.
- [27] The Pierre Auger Collaboration, arXiv:0806.4302 (to be published in *Phys. Rev. Lett.*)
- [28] K. Greisen, *Phys. Rev. Lett.* **16** (1966) 748; G. T. Zatsepin and V. A. Kuz'min, *JETP Lett.* **4** (1966) 78.
- [29] E. Waxman and J. N. Bahcall, *Phys. Rev.* **D59** (1999) 023002.
- [30] J. Ahrens *et al.*, *Astropart. Phys.* **20** (2004) 507; F. Halzen, *Eur. Phys. J.* **C46** (2006) 669; E. Resconi *et al.*, arXiv:0807:3891.